Geochemistry Geophysics Geosystems G3
AN ELECTRONIC JOURNAL OF THE EARTH SCIENCES
Published by AGU and the Geochemical Society

Article
Volume 6, Number 11
10 November 2005
Q11K11, doi:10.1029/2005GC000979
ISSN: 1525-2027

New insights into the origin and distribution of the DUPAL isotope anomaly in the Indian Ocean mantle from MORB of the Southwest Indian Ridge

Christine M. Meyzen
Danish Lithosphere Centre (DLC), Øster Voldgade 10, 1350 Copenhagen, Denmark

Now at Laboratoire de Sciences de la Terre, UMR 5570, Ecole Normale Supérieure de Lyon, 46 Allée d'Italie, F-69364 Lyon Cedex 7, France (christine.meyzen@ens-lyon.fr)

John N. Ludden and Eric Humler
Laboratoire de Géosciences Marines, Institut de Physique du Globe (IPG), 4 Place Jussieu, F-75251 Paris Cedex 05, France (john.ludden@cnrs-dir.fr; humler@ccr.jussieu.fr)

Béatrice Luais
Centre de Recherches Pétrographiques et Géochimiques (CRPG-CNRS), UPR 2300, 15 Rue Notre-Dame-des-Pauvres, BP20, F-54501 Vandoeuvre-Les-Nancy, France (luais@crpg.cnrs-nancy.fr)

Michael J. Toplis
Dynamique Terrestre et Planétaire, UMR 5562, Observatoire Midi-Pyrénées, 14 Avenue Edouard Belin, Toulouse, F-31400 France (toplis@pontos.cst.cnes.fr)

Catherine Mével
Laboratoire de Géosciences Marines, Institut de Physique du Globe (IPG), 4 Place Jussieu, F-75251 Paris Cedex 05, France (mevel@ipgp.jussieu.fr)

Michael Storey
Quaternary Dating Laboratory (QUAD-Lab), Teksam, Building 11.1, Roskilde University Centre, P.O. Box 260, DK-4000 Roskilde, Denmark (storey@ruc.dk)

[1] We report new Sr, Nd, and Pb isotope data for Mid-Ocean Ridge Basalts (MORB) dredged between 35 and 69°E along a ~4100 km section of the Southwest Indian Ridge (SWIR), which is one of the slowest spreading ridges of the global mid-ocean ridge system (full rate of 16 mm yr^{-1}). The SWIR appears isotopically more heterogeneous than other mid-ocean ridges over similar length scales and comparable sampling density. Isotopic variations are generally independent of ridge segmentation, and the degree of heterogeneity decreases from west to east. This decrease in heterogeneity correlates with the observed increase in axial depth and decrease in crustal thickness, commonly attributed to decreasing mantle potential temperature. Data for the easternmost SWIR in the vicinity of the Indian Triple Junction confirm that these lavas are isotopically distinct from those of the Triple Junction, the Southeast Indian Ridge, and the Central Indian Ridge, reflecting the presence of an isotopic boundary over an along-axis distance of less than 78 km. Results for lavas from the 39–41°E section extend the isotopic range of MORB to the lowest $^{206}Pb/^{204}Pb$ values (to 16.58) yet found among oceanic islands and spreading centers worldwide and confirm their extremely anomalously high $^{87}Sr/^{86}Sr$, $^{207}Pb/^{204}Pb$, and $^{208}Pb/^{204}Pb$ and low $^{143}Nd/^{144}Nd$. This extreme Indian signature does not bear any isotopic affinities with recent products of the nearby Marion hot spot. Furthermore, the presence of old subducted marine sediment as a source for the low $^{206}Pb/^{204}Pb$ component is excluded, as no sediment group has the appropriate parent-daughter Th/Pb and U/Pb characteristics to yield such compositions, not even when dewatering subduction processes are considered. Incorporation of old subduction-modified mantle into the MORB source does not yield high enough $^{207}Pb/^{204}Pb$ and $^{208}Pb/^{204}Pb$ to explain the features of lavas from the 39–41°E section. The

unusual isotopic attributes of this section (low $^{206}Pb/^{204}Pb$ and $^{143}Nd/^{144}Nd$ and high $^{87}Sr/^{86}Sr$, $^{207}Pb/^{204}Pb$, and $^{208}Pb/^{204}Pb$) are best explained by the presence of stranded lower continental crust embedded in the upper mantle. This component is also inferred to be present in MORB from other spreading centers in the Indian Ocean.

Components: 17,182 words, 16 figures, 3 tables.

Keywords: Southwest Indian Ridge; MORB; isotopes; Indian Ocean; lower crust; mantle.

Index Terms: 1025 Geochemistry: Composition of the mantle; 1032 Geochemistry: Mid-oceanic ridge processes (3614, 8416); 1040 Geochemistry: Radiogenic isotope geochemistry.

Received 24 March 2005; **Revised** 9 July 2005; **Accepted** 29 August 2005; **Published** 10 November 2005.

Meyzen, C. M., J. N. Ludden, E. Humler, B. Luais, M. J. Toplis, C. Mével, and M. Storey (2005), New insights into the origin and distribution of the DUPAL isotope anomaly in the Indian Ocean mantle from MORB of the Southwest Indian Ridge, *Geochem. Geophys. Geosyst.*, *6*, Q11K11, doi:10.1029/2005GC000979.

Theme: Accretionary Processes Along the Ultra-Slow Spreading Southwest Indian Ridge (SWIR)
Guest Editors: Catherine Mevel and Daniel Sauter

1. Introduction

[2] Over the last twenty years, isotopic studies of Mid-Ocean Ridge Basalts (MORB) have established the existence of a vast mantle isotopic domain in the Indian Ocean, which distinguishes this mantle source from that of the Pacific and north Atlantic [*Dupré and Allègre*, 1983; *Hart*, 1984; *Hamelin and Allègre*, 1985; *Hamelin et al.*, 1986; *Price et al.*, 1986; *Michard et al.*, 1986; *Klein et al.*, 1988; *Dosso et al.*, 1988; *Mahoney et al.*, 1989, 1992, 1996, 1998, 2002; *Pyle et al.*, 1992, 1995; *Kempton et al.*, 2002; *Escrig et al.*, 2004; *Hanan et al.*, 2004]. Along the present Indian ocean spreading axis, this domain includes the entire Central Indian and Carlsberg Ridges, stretching from about 126°E on the Southeast Indian Ridge [*Klein et al.*, 1988; *Pyle et al.*, 1992, 1995], from 26°E on the Southwest Indian Ridge [*Mahoney et al.*, 1992] and northward into the Red Sea [*Schilling et al.*, 1992].

[3] When compared to Atlantic and Pacific MORB, Indian MORB are characterized by distinctly lower $^{206}Pb/^{204}Pb$ and $^{143}Nd/^{144}Nd$ and higher $^{87}Sr/^{86}Sr$, as well as systematically higher $^{207}Pb/^{204}Pb$ and $^{208}Pb/^{204}Pb$ at a given $^{206}Pb/^{204}Pb$ [*Hart*, 1984]. These distinct characteristics have been attributed to the widespread dispersal, in the Indian Ocean mantle of material derived from one or more of the following: (1) Indian ocean hot spot sources, especially from the large long-lived Kerguelen mantle plume [e.g., *Storey et al.*, 1989]; (2) continental lithospheric mantle introduced prior to and/or during the breakup of Gondwana [e.g., *Mahoney et al.*, 1992]; (3) convectively recycled subducted altered oceanic crust and/or sediment [e.g., *Dupré and Allègre*, 1983; *Rekhämper and Hofmann*, 1997]; (4) continental crust from cratonic Gondwanan lithosphere [e.g., *Arndt and Goldstein*, 1989; *Escrig et al.*, 2004; *Hanan et al.*, 2004]; (5) subduction-modified mantle [e.g., *Kempton et al.*, 2002]. Thus, despite its extent, the history and origin of this province are not yet well understood.

[4] In this respect, the Pb-Sr-Nd isotopic compositions of MORB from the Southwest Indian Ridge (SWIR) which is an ultra-slow spreading ridge (full rate <20 mm yr^{-1}) stretching from the Bouvet Triple Junction (55°S, 00°40′W) to the Rodrigues Triple Junction (RTJ, 25°30′S, 70°E) are of particular interest, as they define a gradual isotopic transition in the MORB source mantle from typical Indian Ocean–type composition in the east to Atlantic like ones, west of 26°E [*Mahoney et al.*, 1992]. Nonetheless, previous isotopic studies of MORB from the eastern extremity of the SWIR involve only limited reconnaissance data and sparse sampling along the axis [*Hamelin and Allègre*, 1985; *Michard et al.*, 1986, *Price et al.*, 1986; *Mahoney et al.*, 1989, 1992; *Robinson et al.*, 2001]. The easternmost SWIR section is morphologically an intriguing section as it is characterized by a very deep axial valley (4730 m on average), thick lithosphere and

extremely thin oceanic crust (4–5 km on average) [*Francis and Raitt*, 1967; *Minshull and White*, 1996; *Cannat et al.*, 1999; *Müller et al.*, 1999]. These attributes have been interpreted to reflect a weak magma supply from an underlying mantle which is unusually cold. Previous studies on the easternmost segments of the SWIR mainly investigated the regional provinciality around the Rodrigues Triple Junction (RTJ), and demonstrated that SWIR lavas from the deep eastern extremity differ chemically and isotopically from those of the Southern Central Indian Ridge (CIR), the western Southeast Indian Ridge (SEIR) and the RTJ [*Michard et al.*, 1986; *Price et al.*, 1986; *Mahoney et al.*, 1989; *Meyzen et al.*, 2003]. This provinciality was ascribed either to the eastward progression of a distinct SWIR mantle in response to the migration of the junction [*Mahoney et al.*, 1989] or to sampling of a vertically zoned mantle [*Mahoney et al.*, 1989]. The SWIR eastern extremity near the RTJ was thus identified as a distinct isotopic province although there was no clear definition of its extension to the west.

[5] The central part of the SWIR has been extensively studied [e.g., *LeRoex et al.*, 1989; *Mahoney et al.*, 1992], but most samples were either dredged off-axis or in the transform faults. As a consequence, they did not provide a complete perspective of the along-axis geochemical variations of the SWIR mantle. In this area, the ridge is characterized by a dense network of transform faults and is surrounded by several oceanic islands and aseismic ridges (Prince Edward Island, Marion Island, Funk seamount, Madagascar plateau, Del Cano Rise and Crozet Plateau) marking the locus of the Marion and Crozet hot spots [*Mahoney et al.*, 1992]. One of the most noticeable features of lavas erupted in this area is their large isotopic compositional diversity, which cannot be simply supported by a simple model of ridge-ward flow plumes like those established on faster ridges [*Mahoney et al.*, 1992]. With the exception of the 36–39°E section, near Crozet and Marion Islands, isotopic signatures of MORB show no obvious affinities with those of Marion and Crozet hot spots [*Mahoney et al.*, 1992]. Between 39 and 41°E, basalts exhibit one of the most pronounced Indian Ocean isotope signatures (e.g., low $^{206}Pb/^{204}Pb$ and $^{143}Nd/^{144}Nd$, high $^{207}Pb/^{204}Pb$, $^{208}Pb/^{204}Pb$ and $^{87}Sr/^{86}Sr$ [*Mahoney et al.*, 1992]).

[6] Here, we present new Sr-Nd and Pb isotope data, including the lowest $^{206}Pb/^{204}Pb$ yet observed for oceanic-mantle derived rocks, for basaltic glasses and basalts dredged between 35° and 69°E along the SWIR neovolcanic zone during the SWIFT (winter 2001, R/V *Marion Dufresne*) and EDUL (summer 1997, R/V *Marion Dufresne*) cruises. Our results thus provide a much improved and precise perspective of the along-axis geochemical variations of the SWIR mantle. The precision of the Pb double-spike technique permits a fine scale assessment of the distribution of MORB heterogeneity along the SWIR, in a region where extreme isotope variations provide a key to understanding the distinctive nature of the Indian Ocean mantle.

2. Geological Setting

[7] The SWIR separates the African and Antarctic plates over a distance of ~7700 km, and has been active for more than 100 Ma [*Patriat et al.*, 1997; *Marks and Tikku*, 2001]. In the eastern section sampled for this study (35° to 69°E), the ridge axis is offset by several spectacular long-lived north-south trending transform faults (Figure 1). In its central part, the ridge is surrounded by several oceanic islands and aseismic ridges marking the locus of Marion and Crozet hot spots (Figure 1). Marion Island, which is located at about 250 km south of the ridge axis, marks the current position of the Marion plume. The present-day surface expression of the Crozet hot spot may be either the Crozet archipelago [*Currey and Munasinghe*, 1991] or the Conrad Rise [*Müller et al.*, 1993]. A large regional positive residual geoid anomaly (32–55°E) is centered mid-way between Crozet and Marion Islands [*LeRoex et al.*, 1989]. Between 35 and 69°E seafloor morphology defines four contrasting domains with distinct segmentation styles: a very deep (4730 m) and slightly oblique (25°) domain to the east of the Melville FZ (zone A); a deep (4330 m) and oblique (40°) domain from the Melville FZ to the Gallieni FZ (zone B); a very shallow (3090–3530 m) and oblique domain (40°) from the Gallieni FZ to the Discovery II FZ (Zone C); a shallow (3050 m) and oblique domain west of the Discovery II FZ (zone D) (Figure 1) [*Mendel et al.*, 1997, 2003; *Cannat et al.*, 1999; *Sauter et al.*, 2001]. Within the deepest part of the studied area (zone A), the extremely complex along-axis segmentation pattern is not correlated with the gravimetric segmentation [*Cannat et al.*, 1999], leaving a chaotic off-axis seafloor terrain over the last 20 Myr [*Parson et al.*, 1997; *Patriat et al.*, 1997].

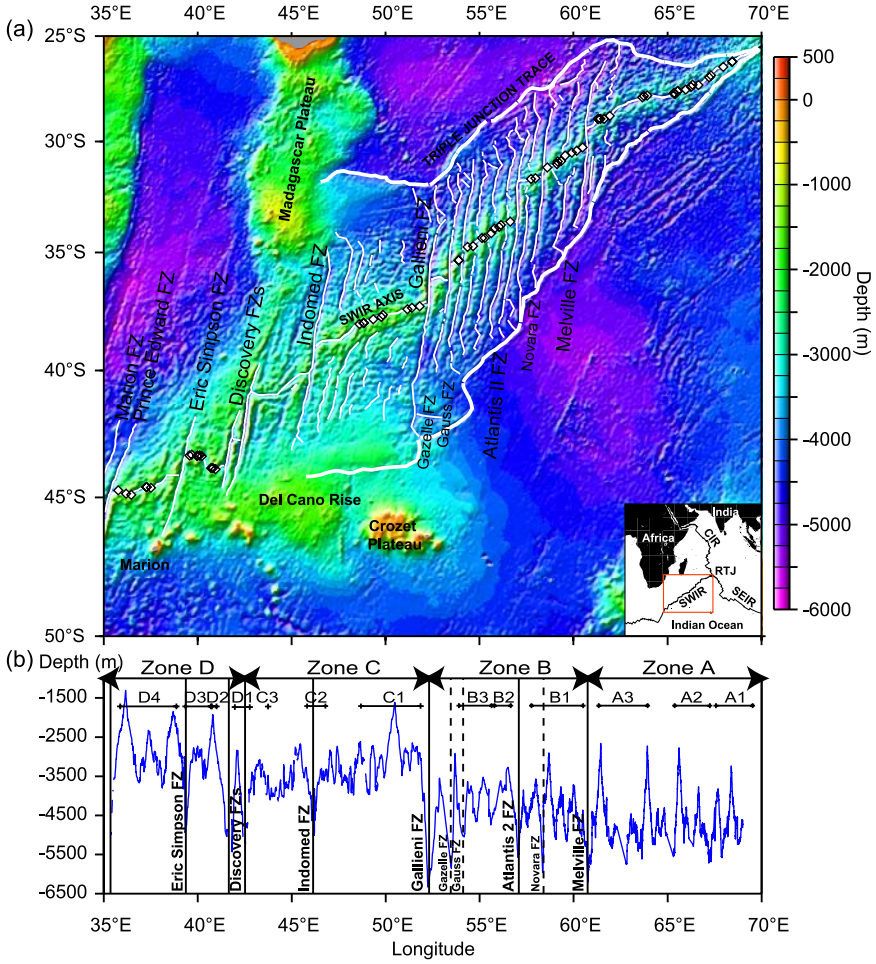

Figure 1. (a) Topographic map of the SWIR from *Smith and Sandwell* [1997] showing sample locations used in this study (open diamonds). (b) Axial bathymetric profile versus longitude (°E) [*Cannat et al.*, 1999; *Mendel et al.*, 2003]. The zones defined by seafloor morphology variations are labeled A-D. Within these zones, isotopic domains are labeled by increasing number going westward. Major (continuous lines) and minor (dashed lines) Fracture Zones (FZ) are also shown. Inset shows regional location of the study area (box): Rodrigues Triple Junction (RTJ), Southeast Indian Ridge (SEIR), and Central Indian Ridge (CIR).

These features have been ascribed to either episodic but intense volcanic activity [*Cannat et al.*, 1999], to restricted and intermittent mantle diapirism [*Mendel et al.*, 1997], or to the temporal evolution of the RTJ configuration [*Patriat et al.*, 1997]. The presence of rare very high volcanic constructions (maximum height: 2672 m above seafloor) requires the presence of a thick lithosphere [*Cannat et al.*, 1999]. In contrast, between the Gallieni and Atlantis II FZ, the axial segmentation pattern is well defined and broadly continuous over the past 40 Myr [*Sauter et al.*, 2001]. To the west of the Gallieni FZ (zone C), as observed for zone A, the along-axis segmentation leaves no clear off-axis trace for the last 15 Myr. This change of segmentation pattern, either side of the Gallieni FZ, has been attributed to the temporal evolution of the RTJ configuration [*Sauter et al.*, 2001]. Within zone C, mean axial depth is greater and segments are shorter than to the west of the Discovery FZ [*Mendel et al.*, 2003]. Between the Indomed FZ (46°E) and Gallieni FZ (52°20′E), the presence of axial bathymetric highs and gravity lows reflect either remnant effects of the Del Cano Rise or excess volcanism due to the off-axis Crozet plume [*Georgen et al.*, 2001]. Within zone D, between the Andrew Bain FZ (32°18′E) and Discovery II FZ, evidence for an interaction of the ridge with the Marion hot spot is provided by pronounced axial gravity lows and shallow axial depth over 1100 km [*Georgen et al.*, 2001; *Georgen and Lin*, 2003]. Off-axis, these gravity lows extend from Marion Island

Table 1. Sr, Nd, and Pb Isotopic Data for SWIR Basalts and Basaltic Glasses, 35°–69°E[a]

Sample	Lat., °S	Long., °E	Depth, m	Zone	$^{206}Pb/^{204}Pb$	2σ	$^{207}Pb/^{204}Pb$	2σ	$^{208}Pb/^{204}Pb$	2σ	$^{87}Sr/^{86}Sr$	$^{143}Nd/^{144}Nd$
ED-DR1-1-1	26.10	68.73	4775	A1	18.1419	0.0008	15.4664	0.0009	37.9818	0.0019	*0.702964*	*0.513034*
					18.1426	0.0009	15.4674	0.0009	37.9857	0.0020	-	-
					18.1441	**0.0025**	**15.4691**	**0.0024**	**37.9934**	**0.0058**	-	-
ED-DR2 Glass stn	26.23	68.44	3755	A1	17.9841	0.0021	15.4557	0.0018	37.7952	0.0045	*0.702914*	0.513068
					-	-	-	-	-	-	-	0.513103
ED-DR2-1-1	26.23	68.44	3755	A1	17.9881	0.0017	15.4594	0.0018	37.8052	0.0041	*0.702954*	*0.513042*
ED-DR3-2-1	26.49	67.98	4750	A1	**17.9716**	**0.0015**	**15.4580**	**0.0014**	**37.8186**	**0.0033**	*0.702896*	0.513069
					17.9731	0.0020	15.4583	0.0019	37.8183	0.0046	-	*0.513047*
ED-DR5 Glass stn	26.89	67.32	4113	A2	-	-	-	-	-	-	*0.702867*	*0.513062*
ED-DR6-4-1	26.98	67.23	4700	A2	17.8906	0.0028	15.4585	0.0028	37.8276	0.0065	*0.703120*	0.513015
ED-DR7-2-5	27.35	66.65	3725	A2	18.0735	0.0011	15.4831	0.0011	38.0759	0.0024	*0.703234*	*0.513013*
ED-DR8-2	27.34	66.34	4375	A2	17.7783	0.0009	15.4410	0.0008	37.6898	0.0020	*0.702966*	0.513050
					17.7814	0.0022	15.4444	0.0020	37.6998	0.0048	*0.702924*	*0.513079*
					17.7742	*0.0004*	*15.4341*	*0.0003*	*37.6729*	*0.0010*	-	-
ED-DR9-3-1	27.44	66.26	4350	A2	17.9184	0.0014	15.4583	0.0014	37.8354	0.0032	*0.703122*	*0.513018*
					17.9121	*0.0004*	*15.4551*	*0.0005*	*37.8351*	*0.0014*	-	-
ED-DR10-1-4	27.57	65.98	4310	A2	17.8274	0.0014	15.4469	0.0014	37.7084	0.0032	0.702889	0.513065
ED-DR11-1-9	27.63	65.54	3475	A2	18.0417	0.0008	15.4971	0.0008	38.1582	0.0017	0.703626	0.512885
					18.0385	0.0021	15.4936	0.0020	38.1459	0.0046	*0.703610*	*0.512859*
					18.0404	*0.0006*	*15.5019*	*0.0005*	*38.1774*	*0.0015*	-	-
ED-DR11-1-2	27.63	65.54	3475	A2	**18.0428**	**0.0022**	**15.4991**	**0.0036**	**38.1612**	**0.0073**	**0.703626**	**0.512911**
ED-DR12-1-2	27.74	65.35	5375	A2	17.8909	0.0009	15.4538	0.0009	37.8097	0.0020	*0.702916*	0.513080
					17.8859	0.0034	15.4488	0.0028	37.7940	0.0067	-	*0.513067*
					17.8881	**0.0018**	**15.4515**	**0.0017**	**37.8028**	**0.0042**	-	-
					17.8870	*0.0006*	*15.4529*	*0.0007*	*37.8114*	*0.0020*	-	-
ED-DR12-3-2	27.74	65.35	5375	A2	17.8856	0.0019	15.4480	0.0019	37.7925	0.0054	*0.702941*	0.513042
					17.8841	0.0024	15.4460	0.0022	37.7854	0.0053	*0.702944*	*0.513007*
					-	-	-	-	-	-	0.702904	-
ED-DR13 tube	27.78	65.42	5175	A2	17.8093	0.0009	15.4487	0.0018	37.7479	0.0029	*0.703052*	0.513027
					17.8109	0.0016	15.4486	0.0015	37.7468	0.0038	*0.703078*	*0.513037*
ED-DR16 Tube	27.85	63.92	2850	A3	17.7976	0.0016	15.4343	0.0016	37.6335	0.0044	*0.702777*	0.513069
ED-DR19-1-3	27.86	63.75	4475	A3	17.8003	0.0010	15.4348	0.0011	37.6637	0.0021	*0.702795*	-
					17.7962	*0.0006*	*15.4289*	*0.0006*	*37.6485*	*0.0018*	*0.702819*	-
ED-DR20-1-1	27.93	63.66	4675	A3	18.0280	0.0027	15.4664	0.0026	37.8453	0.0064	0.702710	0.513152
					18.0283	0.0079	15.4642	0.0075	37.8426	0.0184	-	-
ED-DR26-1	28.80	61.93	4520	A3	17.9929	0.0071	15.4874	0.0063	37.9842	0.0156	*0.702868*	0.513055
ED-DR27 tube	28.94	61.64	4375	A3	17.9282	0.0035	15.4535	0.0035	37.7838	0.0081	0.702748	0.513108
					-	-	-	-	-	-	-	0.513148
ED-DR28-2-5	28.95	61.44	2750	A3	**17.7461**	**0.0015**	**15.4337**	**0.0014**	**37.5893**	**0.0033**	*0.702747*	*0.513123*
ED-DR29-1-1	28.95	61.32	3550	A3	**17.6819**	**0.0027**	**15.4307**	**0.0026**	**37.5406**	**0.0062**	0.702749	0.513097
					17.6790	0.0031	15.4280	0.0027	37.5321	0.0066	*0.702755*	*0.513104*
ED-DR29-1-2	28.95	61.32	3550	A3	**17.6775**	**0.0017**	**15.4279**	**0.0016**	**37.5334**	**0.0037**	**0.702721**	**0.513092**
ED-DR32-4-4	30.27	60.49	4450	B1	**17.4498**	**0.0020**	**15.4023**	**0.0020**	**37.1346**	**0.0045**	**0.702749**	**0.513172**
ED-DR34-1-3	30.43	60.16	4450	B1	17.4023	0.0010	15.3962	0.0012	37.0778	0.0023	*0.702659*	*0.513215*
					17.4052	0.0014	15.3976	0.0017	37.0816	0.0036	-	-
ED-DR35 pot4	30.52	59.91	4250	B1	17.4018	0.0014	15.4006	0.0014	37.1097	0.0038	0.702911	0.513125
	30.52	59.91	4250	B1	-	-	-	-	-	-	*0.702953*	*0.513118*
ED-DR36 Tube	30.66	59.56	4350	B1	17.4323	0.0012	15.4014	0.0012	37.1355	0.0032	0.702774	0.513160
					17.4320	0.0013	15.4005	0.0013	37.1335	0.0035	-	0.513130
					-	-	-	-	-	-	-	*0.513129*
ED-DR38-1-1	30.91	59.33	3875	B1	17.4224	0.0013	15.4013	0.0013	37.1104	0.0029	0.702829	0.513134
					-	-	-	-	-	-	-	*0.513178*
ED-DR41-1-1	30.92	59.16	4275	B1	17.3631	0.0013	15.3923	0.0012	37.0698	0.0029	*0.702824*	*0.513157*

Table 1. (continued)

Sample	Lat., °S	Long., °E	Depth, m	Zone	$^{206}Pb/^{204}Pb$	2σ	$^{207}Pb/^{204}Pb$	2σ	$^{208}Pb/^{204}Pb$	2σ	$^{87}Sr/^{86}Sr$	$^{143}Nd/^{144}Nd$
ED-DR42 glass stn	31.05	59.12	4500	B1	17.4040	0.0010	15.3980	0.0012	37.0847	0.0035	*0.702723*	0.513167
					17.4032	0.0011	15.3966	0.0013	37.0818	0.0039	-	*0.513143*
ED-DR46-1-6	31.19	58.61	4050	B1	17.4290	0.0035	15.3963	0.0034	37.1141	0.0081	0.702707	0.513170
ED-DR48 Tube	31.69	57.97	3600	B1	17.5354	0.0010	15.4181	0.0011	37.2715	0.0030	*0.702950*	0.513096
					17.5312	0.0014	15.4134	0.0016	37.2579	0.0034	-	-
ED-DR49 pot	31.73	57.74	3975	B1	17.4960	0.0019	15.4134	0.0019	37.2152	0.0043	0.702851	0.513134
					-	-	-	-	-	-	0.702861	-
ED-DR51-1-1	33.65	56.64	3675	B2	**17.9864**	**0.0018**	**15.4730**	**0.0017**	**37.6813**	**0.0040**	0.702822	0.513073
					17.9835	0.0030	15.4698	0.0028	37.6726	0.0069	-	-
ED-DR 52 Glass stn	33.79	56.13	3550	B2	18.1278	0.0020	15.4867	0.0020	37.7668	0.0056	0.702732	0.513097
					18.1315	0.0050	15.4885	0.0046	37.7737	0.0112	*0.702763*	*0.513050*
					-	-	-	-	-	-	*0.702746*	-
ED-DR53-2-3	33.87	56.03	3150	B2	18.0786	0.0026	15.4773	0.0024	37.7434	0.0060	0.702658	0.513122
ED-DR55-2-1	33.96	55.78	3735	B2	17.8978	0.0010	15.4733	0.0011	37.6445	0.0023	*0.703177*	**0.513037**
					17.8969	0.0010	15.4720	0.0011	37.6405	0.0023	**0.703173**	-
					17.8968	**0.0013**	**15.4727**	**0.0012**	**37.6537**	**0.0029**	-	-
ED-DR57-1-1	34.15	55.63	4100	B3	**18.1598**	**0.0035**	**15.4969**	**0.0032**	**37.9394**	**0.0078**	0.702907	0.513072
					18.1586	0.0084	15.4967	0.0078	37.9344	0.0191	-	-
ED-DR60 glass stn	34.37	55.26	3650	B3	17.8398	0.0012	15.4596	0.0013	37.7016	0.0037	0.702943	0.513016
					-	-	-	-	-	-	*0.702963*	*0.513010*
ED-DR61-2-4	34.36	55.13	3650	B3	**17.8931**	**0.0013**	**15.4613**	**0.0011**	**37.7300**	**0.0028**	0.702916	**0.513038**
					-	-	-	-	-	-	**0.702916**	-
ED-DR63-1	34.73	54.65	3800	B3	17.7754	0.0009	15.4535	0.0009	37.6722	0.0025	0.702956	0.513054
					17.7731	0.0013	15.4508	0.0015	37.6654	0.0031	*0.702962*	0.513077
					-	-	-	-	-	-	-	*0.513063*
ED-DR66	34.76	54.37	3725	B3	18.1221	0.0028	15.4854	0.0026	37.9595	0.0061	0.702882	0.513081
ED-DR68 Tube	35.34	53.89	4050	B3	17.6015	0.0010	15.4278	0.0013	37.5365	0.0035	*0.702973*	0.513070
					17.6044	0.0017	15.4286	0.0015	37.5348	0.0038	-	-
ED-DR68-1	35.34	53.89	4050	B3	17.6024	0.0025	15.4273	0.0005	37.5315	0.0011	*0.702967*	0.513088
					-	-	-	-	-	-	-	*0.513082*
ED-DR70-1-1	37.33	51.81	2875	C1	18.1003	0.0046	15.4952	0.0042	37.9263	0.0102	*0.702987*	0.513154
					-	-	-	-	-	-	-	*0.513128*
ED-DR71	37.39	51.39	2750	C1	18.2224	0.0023	15.5073	0.0021	38.0605	0.0056	0.703067	0.513109
ED-DR72 Glass stn	37.46	51.16	2800	C1	18.2028	0.0019	15.5012	0.0019	38.0262	0.0045	0.703044	0.513104
					18.2019	0.0017	15.5009	0.0017	38.0220	0.0047	*0.703014*	*0.513108*
ED-DR73-2	37.69	49.85	2800	C1	18.2260	0.0052	15.4904	0.0047	37.9952	0.0116	*0.702722*	0.513120
ED-DR76 Glass stn	37.79	49.77	2300	C1	-	-	-	-	-	-	*0.702819*	*0.513111*
ED-DR75-1-1	37.87	49.34	2775	C1	**18.1444**	**0.0022**	**15.4871**	**0.0020**	**37.9598**	**0.0051**	*0.702923*	**0.513171**
SW-DR32-1-1	38.03	48.83	2760	C1	18.1611	0.0021	15.4888	0.0020	37.9769	0.0047	0.702934	0.513166
SW-DR32-1-3	38.03	48.83	2760	C1	18.1656	0.0027	15.4922	0.0030	37.9851	0.0089	0.702887	0.513168
SW-DR30-1-4	38.08	48.62	2760	C1	18.1438	0.0034	15.4948	0.0037	37.9911	0.0033	0.703157	0.513139
SW-DR20-1-1	43.92	40.94	2700	D2	18.4067	0.0014	15.5268	0.0014	38.1741	0.0035	0.702994	0.513037
					18.4048	0.0013	15.5249	0.0014	38.1690	0.0036	0.702993	-
					18.4061	0.0017	15.5262	0.0016	38.1730	0.0044	-	-
SW-DR19-1-6	43.89	40.81	1970	D2	18.4122	0.0027	15.5253	0.0025	38.1444	0.0068	0.703008	0.513089
SW-DR17-1-3	43.89	40.70	2550	D2	18.4256	0.0020	15.5250	0.0018	38.1687	0.0047	0.702923	0.513005
					18.4263	0.0021	15.5262	0.0021	38.1701	0.0054	0.702929	-
SW-DR15-2-5	43.43	40.21	3000	D3	17.1577	0.0016	15.4302	0.0017	37.3632	0.0043	0.703905	0.512861
SW-DR14-1-4	43.40	40.10	2770	D3	17.2726	0.0018	15.4409	0.0018	37.4083	0.0048	0.703717	0.512871
					17.2738	0.0021	15.4427	0.0022	37.4116	0.0063	0.703718	-
SW-DR13-1-2	43.41	39.98	2880	D3	16.5850	0.0020	15.3599	0.0021	36.8753	0.0055	0.704761	0.512607
					16.5850	0.0020	15.3599	0.0021	36.8753	0.0055	0.704769	-
SW-DR13-1-19	43.41	39.98	2880	D3	16.5826	0.0023	15.3558	0.0024	36.8665	0.0059	0.704746	-
SW-DR10#3	43.36	39.69	3120	D3	17.2434	0.0026	15.4496	0.0025	37.4273	0.0058	0.703938	0.512870

Table 1. (continued)

Sample	Lat., °S	Long., °E	Depth, m	Zone	$^{206}Pb/^{204}Pb$	2σ	$^{207}Pb/^{204}Pb$	2σ	$^{208}Pb/^{204}Pb$	2σ	$^{87}Sr/^{86}Sr$	$^{143}Nd/^{144}Nd$
					-	-	-	-	-	-	0.703930	-
SW-DR16-3-3	43.43	40.21	3100	D3	17.2033	0.0015	15.4382	0.0016	37.4102	0.0045	0.703863	0.512863
SW-DR9-1-3	44.63	37.50	2730	D4	18.2269	0.0037	15.4992	0.0036	37.9639	0.0090	0.702788	-
SW-DR8-2-1	44.61	37.27	2850	D4	18.3562	0.0024	15.5229	0.0023	38.1451	0.0062	0.702960	0.513138
SW-DR8-2-3	44.61	37.27	2850	D4	18.3469	0.0033	15.5066	0.0030	38.1260	0.0079	0.703134	-
SW-DR6-2-2	44.90	36.47	2400	D4	18.2890	0.0020	15.5095	0.0018	38.0463	0.0050	0.702882	0.513147
SW-DR5-1-2	44.86	36.18	1320	D4	18.3663	0.0012	15.5162	0.0012	38.1243	0.0032	0.702915	0.513102
SWR-DR4-1-2	44.73	35.78	2750	D4	18.2423	0.0017	15.5023	0.0017	37.9802	0.0045	-	0.513179

[a] Samples are designated as W-X-Y-Z, indicating cruise (ED: EDUL, SW: SWIFT), dredge, sample type for each dredge, and block numbers. SWIR basalt data are in bold. All Pb, Sr, and Nd measurements in italic were made at the Centre de Recherches Pétrographiques et Géochimiques (CRPG-CNRS, France). Data were also acquired at the Danish Lithosphere Centre (DLC, Denmark) and the Geological Institute, University of Copenhagen (GI, Denmark). All basaltic chips and glasses were respectively leached in hot 6N HCl for 30 and 10 min at 120°C, followed by brief ultrasonic leaching in Milli-Q water. For Pb analysis performed at DLC and CRPG, Pb was extracted according to the techniques of *Baker et al.* [2004] and *Manhès et al.* [1978], respectively. Blanks on a 100 mg sample were less than 5–10 pg at DLC. They were less than 100 pg on 300 mg sample at CRPG. Blanks for Sr and Nd were found to be negligible. Double-spike (DS) Pb and Nd measurements performed on an MC-ICP-MS (AXIOM) at DLC follow the procedure of *Baker et al.* [2004] and *Luais et al.* [1997]. The $^{207}Pb-^{204}Pb$ double spike used is SBL7/4 and was prepared by Rex Taylor (University of Southampton, UK) and Laure Dosso (University of Brest, France). The average value for SRM981 obtained on repeated runs (N = 11) is 16.9410 ± 0.0032 (2 sd) for $^{206}Pb/^{204}Pb$, 15.4990 ± 0.0033 for $^{207}Pb/^{204}Pb$, and 36.7250 ± 0.0085 for $^{208}Pb/^{204}Pb$. The within-run uncertainty of the sample ED-DR57-1-1 is considered to represent the uncertainties on the Pb measurements. The Nd isotope measurements of standards are $^{143}Nd/^{144}Nd$ = 0.512131 ± 0.000023 (N = 29, Ames) and $^{143}Nd/^{144}Nd$ = 0.511844 ± 0.000026 (N = 10, La Jolla). Pb-isotope measurements acquired on the Isoprobe MC-ICPMS at CRPG were exponentially corrected for mass fractionation using the Tl-doping method [*Rehkämper and Mezger*, 2000; *White et al.*, 2000] with a Pb/Tl = 10 and a constant $^{203}Tl/^{205}Tl$ value of 2.38714 [*Dunstan et al.*, 1980]. All Pb isotopic values have been normalized to the SRM981 composition of *Todt et al.* [1996]. The mean values for SRM981 (N = 37) are 16.9319 ± 0.0032 (2 sd) for $^{206}Pb/^{204}Pb$, 15.4899 ± 0.0038 for $^{207}Pb/^{204}Pb$, and 36.7014 ± 0.0118 for $^{208}Pb/^{204}Pb$. For Sr isotopes acquired on a Thermo-Ionization Mass Spectrometer (TIMS) VG Sector 54-IT at the GI, the mean $^{87}Sr/^{86}Sr$ value of SRM987 standard is 0.710241 ± 0.000028 (N = 4). For Nd and Sr isotope analyses, which were performed on a TIMS Finnigan MAT 262 at CRPG, the mean isotope standards for $^{87}Sr/^{86}Sr$ and $^{143}Nd/^{144}Nd$ are 0.710164 ± 28 (N = 15, SRM 987) and 0.511096 ± 26 (N = 16, Johnson Matthey), respectively.

to the Madagascar plateau, which is considered as being the Late Cretaceous-Tertiary trace of the Marion hot spot on the African plate [*Storey et al.*, 1995; *Georgen et al.*, 2001].

3. Results

3.1. Pb, Sr, and Nd Isotope Domains Within the SWIR Mantle

[8] Samples were obtained during the EDUL (R/V *Marion Dufresne*, summer 1997) and SWIFT (R/V *Marion Dufresne*, winter 2001) cruises (Table 1). 113 dredge sites were selected along ~4100 km of the SWIR between (26.10°S, 68.73°E) and (47.13°S, 32.48°E), along the neovolcanic zone (Figure 1). Geochemical data and analytical techniques are given in Table 1.

3.1.1. General Trends

[9] When plotted as a function of longitude (Figure 2), our new results combined with data from the literature for the SWIR provide an excellent overview of the general patterns of mantle heterogeneity along this ridge. Our data generally overlap those of earlier studies obtained without the double-spike (DS) technique for Pb isotopes [e.g., *Mahoney et al.*, 1989, 1992], with the exception of some older $^{207}Pb/^{204}Pb$ data [e.g., *Price et al.*, 1986]. The SWIR data cover a wide range of isotopic compositions, encompassing a substantial fraction of the range seen in MORB from all oceans (Table 1, Figure 2); $^{206}Pb/^{204}Pb$ varies from 16.583 to 18.426; $^{87}Sr/^{86}Sr$ from 0.7027 to 0.7048; $^{143}Nd/^{144}Nd$ from 0.5126 to 0.5132. Most of the isotopic range over the studied region is represented by small-scale variations (Figure 2). For example, the isotopic heterogeneity of lavas located between 39 and 41°E (group D3) is remarkable, although it should be noted that the heterogeneity in Nd-Sr-Pb isotopes at the scale of an individual dredge is negligible (e.g., SW-DR13).

[10] To the east of the Gallieni FZ, the general shapes of the isotopic patterns for Pb, and to a lesser extent for Nd, correlate well with physical discontinuities, but not with variations in seafloor topography (Figures 1 and 2). There is generally no continuity in terms of Nd and Pb-isotopic composition across the major ridge offsets (>90 km), while the Sr isotope profile is more uniform. In contrast, to the west of the Gallieni FZ, the patterns are different with lavas erupted in the vicinity of certain long-offset transforms (Eric Simpson and Indomed FZs) having lower $^{143}Nd/^{144}Nd$, higher $^{87}Sr/^{86}Sr$ and Δ8/4 (the offset of $^{208}Pb/^{204}Pb$ rela-

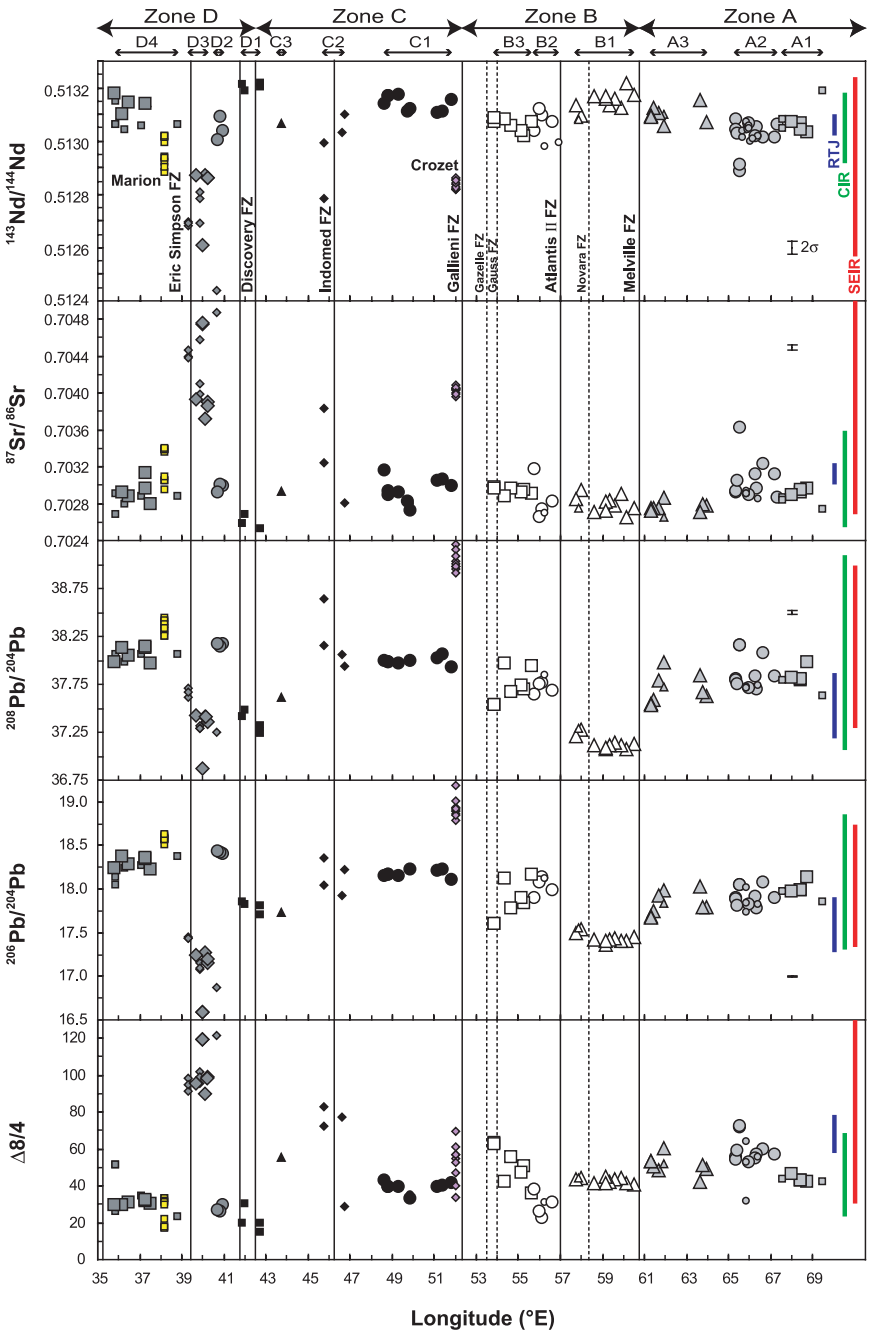

Figure 2. Along-axis profiles of isotope ratios from the SWIR lavas between 35° and 69°E. Data from this study are shown as big symbols along with 2σ error bars. Previous data (small symbols) for the SWIR are from *Dupré and Allègre* [1983], *Hamelin and Allègre* [1985], *Michard et al.* [1986], *Price et al.* [1986], *Mahoney et al.* [1989, 1992], and *Robinson et al.* [2001]. Data for Marion and Crozet hot spots are from *Hart* [1988] and *Mahoney et al.* [1992, 1996]. Solid bars on right-hand side represent the range of isotope variations reported for Southeast Indian Ridge (SEIR), Central Indian Ridge and Carlsberg Ridge (CIR), and Rodrigues Triple Junction (RTJ) MORB [*Hamelin et al.*, 1986; *Michard et al.*, 1986; *Price et al.*, 1986; *Ito et al.*, 1987; *Dosso et al.*, 1988; *Klein et al.*, 1988; *Mahoney et al.*, 1989, 1992; *Pyle et al.*, 1992, 1995; *Schiano et al.*, 1997; *Rëkhamper and Hofmann*, 1997; *Kempton et al.*, 2002]. Data sets include both whole rock and glasses analyses. Locations of the major (continuous lines) and minor (dashed lines) Fracture Zones (FZ) are also shown.

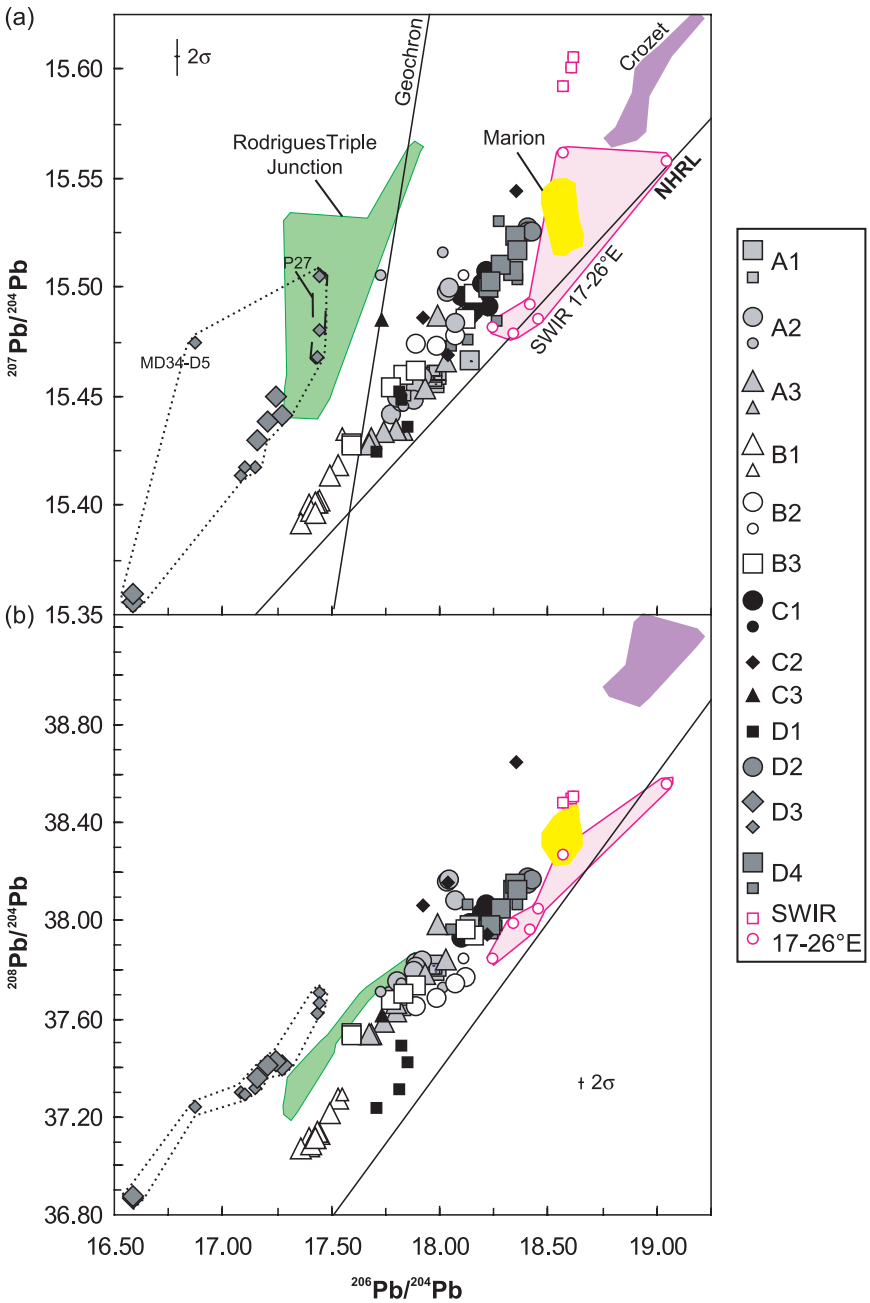

Figure 3. (a) $^{207}Pb/^{204}Pb$ and (b) $^{208}Pb/^{204}Pb$ against $^{206}Pb/^{204}Pb$ for SWIR lavas. Error bar is for data in this study. Big symbols represent SWIR MORBs from this study; small symbols are previous data. Data sources as in Figure 2. Shaded fields are for RTJ [*Price et al.*, 1986; *Michard et al.*, 1986; *Ito et al.*, 1987], Marion [*Hart*, 1988; *Mahoney et al.*, 1992], and Crozet [*Mahoney et al.*, 1996] hot spots and SWIR MORB of south Atlantic affinity located between 17 and 26°E [*Mahoney et al.*, 1992]. Within this latter area, three samples from the Du Toit FZ (pink squares) are isotopically anomalous and have been interpreted as being erratics from the South Sandwich Islands [*Mahoney et al.*, 1992]. NHRL denotes the Northern Hemisphere Reference Line [*Hart*, 1984].

tive to the Northern Hemisphere reference line at a given $^{206}Pb/^{204}Pb$, as defined by [*Hart*, 1984]). In detail, the long and small length-scale variations of different isotopic ratios differ significantly from each other. For example, the high Nd and low Pb isotope values between 57 and 61°E are not correlated with Sr-isotope variations.

[11] Over the area studied, the ridge may interact with either the Marion hot spot at ~38°E or the

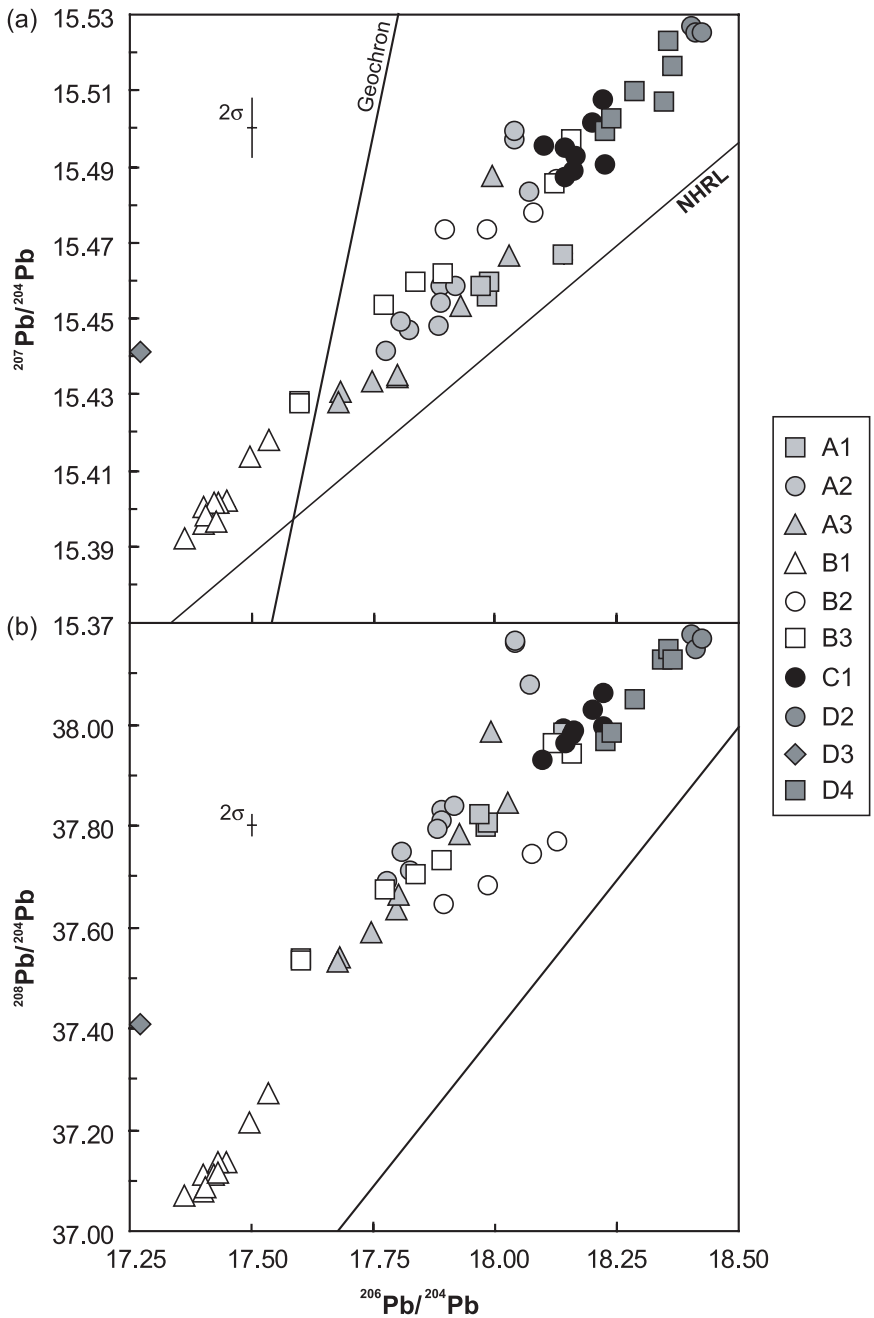

Figure 4. Close-up of the (a) $^{207}Pb/^{204}Pb$ and (b) $^{208}Pb/^{204}Pb$ against $^{206}Pb/^{204}Pb$ variations of SWIR lavas from this study.

Crozet hot spot at ~52°E, as suggested by gravimetric and bathymetric data [*Georgen et al.*, 2001; *Georgen and Lin*, 2003]. Geographically, the 39–41°E section (groups D2–D3) roughly corresponds to the intersection of the ridge with the southern extension of the Madagascar Rise, which is the presumed post–80 Ma trace of the Marion hot spot on the African plate (Figures 1 and 2) [*Storey et al.*, 1995]. Importantly, Marion hot spot lack Indian Ocean isotope attributes and is characterized by extremely low values of Δ8/4 (16.8–32.9) [*Hart*, 1988; *Mahoney et al.*, 1992]. It falls partially below the threshold between Pacific and Indian mantle (Δ8/4 < 20, whereas Δ8/4 is >20 for virtually all Indian MORB [*Mahoney et al.*, 2002]). Another feature is that it has more MORB-like rather than ocean-island like isotope attributes (Figures 2, 3, 5, and 7). This particularity may account for the

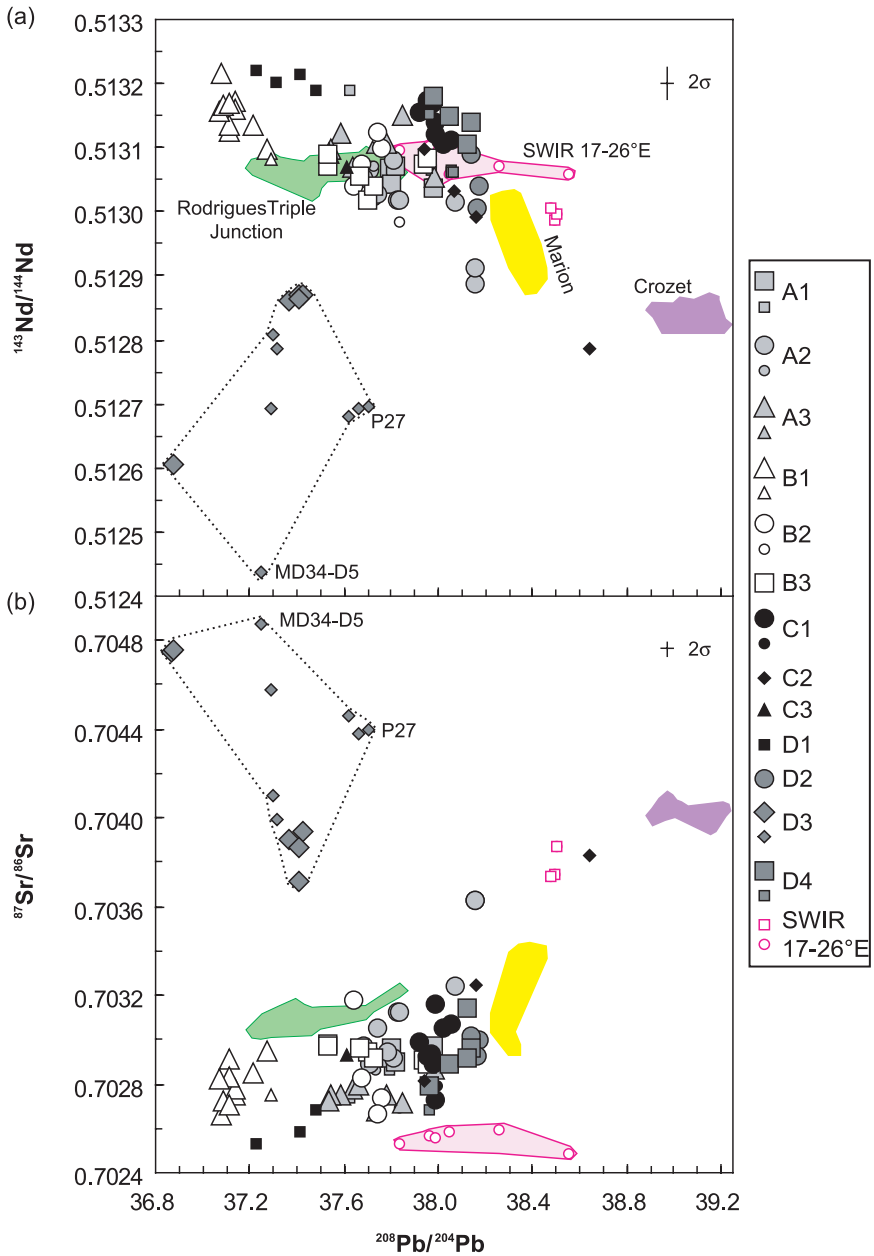

Figure 5. (a) $^{143}Nd/^{144}Nd$ and (b) $^{87}Sr/^{86}Sr$ against $^{208}Pb/^{204}Pb$ for SWIR lavas. Error bar is for data in this study. Big symbols represent SWIR MORBs from this study; small symbols are previous data. Data sources as in Figure 2.

absence of large-scale or small-scale gradients occurring in the vicinity of its potential on-axis location in the along-axis isotopic profiles (Figure 2). In contrast, the influence of Crozet hot spot should lead to increasing $^{87}Sr/^{86}Sr$, $^{206}Pb/^{204}Pb$, $^{207}Pb/^{204}Pb$, $^{208}Pb/^{204}Pb$ and decreasing $^{143}Nd/^{144}Nd$ in the vicinity of ~52°E. This is not observed (Figure 2) and the long ridge-hot spot conduit of more than 1000 km from the Crozet plateau to the SWIR (Figure 1) makes it unlikely that this hot spot influence would be present on the SWIR.

[12] For the SWIR, if the isotopic excursions near the Eric Simpson Fracture Zone (group D3) and Indomed FZ (group C2) are removed, systematic east-west variations are observed, as noted by *Mahoney et al.* [1992]. This is best expressed by the parameter Δ8/4, and to a lesser extent $^{206}Pb/^{204}Pb$ (Figure 2). To the west of the Gallieni FZ, there is a general eastward increase in Δ8/4, but this increase is extremely irregular, resulting in large variations over small length scales such as between the Discovery FZ complex and Eric

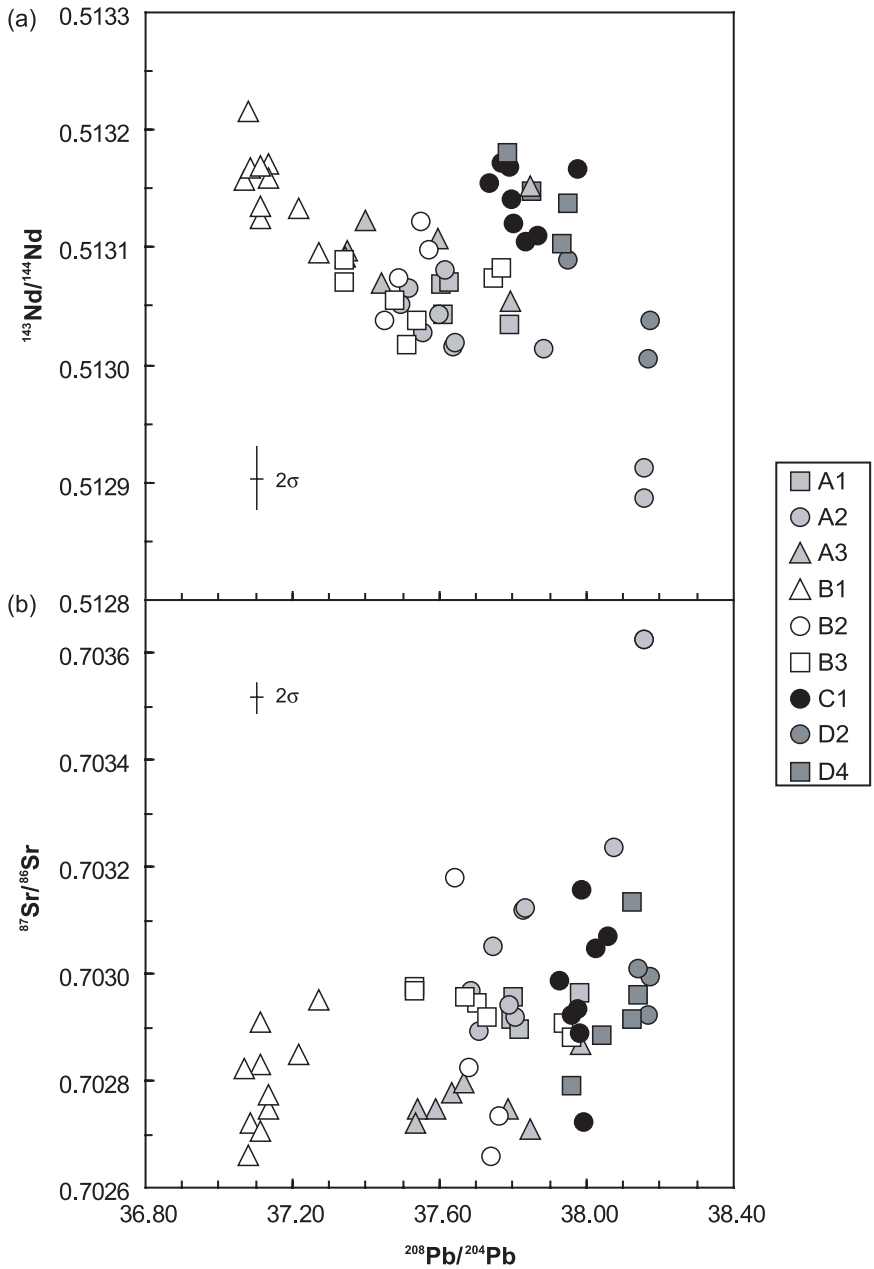

Figure 6. Close-up of the (a) $^{143}Nd/^{144}Nd$ and (b) $^{87}Sr/^{86}Sr$ against $^{208}Pb/^{204}Pb$ variations of SWIR lavas from this study.

Simpson FZ (25.7–119.7) and in the vicinity of the Indomed FZ (28.6–83.1). These anomalies, which are a dominant feature of the regional trend, appear to become less pronounced from the west to the east, at least to the east of the Indomed FZ.

3.1.2. Isotopic Domains

[13] As observed for other Indian mid-ocean ridges, correlations between $^{208}Pb/^{204}Pb$ and $^{143}Nd/^{144}Nd$, $^{208}Pb/^{204}Pb$ and $^{87}Sr/^{86}Sr$ are poor (r = −0.46 and 0.49), but are good between Pb isotope pairs (r = 0.95–0.98, Table 2, Figures 3 and 4). In detail, the Pb correlations are composed of numerous groups or arrays defined by geographically related samples over a few degrees of longitude (Figures 3 and 4).

[14] On the basis of trace and major element characteristics of SWIR basaltic glasses, *Meyzen et al.* [2003] subdivided the area between 49 and 69°E into two main provinces (e.g., zones A and B) separated by the Melville FZ. However, in zones A and B, six different isotopic domains

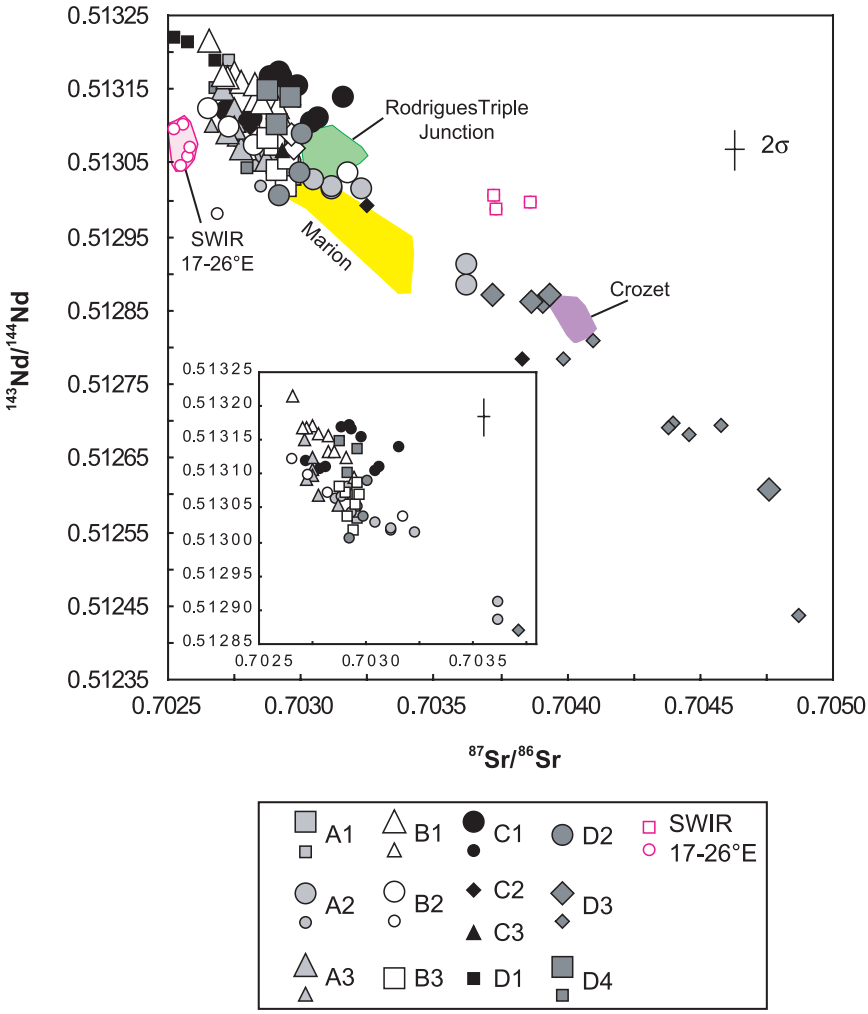

Figure 7. $^{143}Nd/^{144}Nd$ against $^{87}Sr/^{86}Sr$ for SWIR lavas. Big symbols represent SWIR MORBs from this study; small symbols are previous data. Data sources as in Figure 2. Inset shows our SWIR data.

(A1–A3 and B1–B3) can be defined (Figures 1b–4). Within zone A, for the same range of $^{206}Pb/^{204}Pb$, MORB from the section A2 are characterized by higher $^{208}Pb/^{204}Pb$, $^{87}Sr/^{86}Sr$ and lower $^{143}Nd/^{144}Nd$ than those from the adjacent sections A1 and A3 (Figures 3–6), with a broad negative correlation between $^{87}Sr/^{86}Sr$ and $^{143}Nd/^{144}Nd$ (Figure 7). Samples from the section A1, closest to the RTJ, have lower $^{207}Pb/^{204}Pb$, $^{208}Pb/^{204}Pb$ and $^{87}Sr/^{86}Sr$ ratios than the fields defined by the RTJ basalts (Figures 3–5).

[15] Within zone B, the section B1, bounded by the Melville FZ and Atlantis II FZ, is remarkable

Table 2. Correlation of Isotope Ratios in SWIR MORB (N = 56)[a]

	$^{206}Pb/^{204}Pb$	$^{207}Pb/^{204}Pb$	$^{208}Pb/^{204}Pb$	$^{87}Sr/^{86}Sr$	$^{143}Nd/^{144}Nd$
$^{206}Pb/^{204}Pb$	1	0.977	0.951	0.307	−0.269
$^{207}Pb/^{204}Pb$	0.977	1	0.949	0.419	−0.322
$^{208}Pb/^{204}Pb$	0.951	0.949	1	0.494	−0.461
$^{87}Sr/^{86}Sr$	0.307	0.419	0.494	1	−0.726
$^{143}Nd/^{144}Nd$	−0.269	−0.322	−0.461	−0.726	1

[a] Excluding those of the 39–41°E section, which trend obliquely compared to the main SWIR population. Only samples where all the ratios were available have been used.

in its very low $^{206}Pb/^{204}Pb$ (down to 17.363), and low $^{207}Pb/^{204}Pb$, $^{208}Pb/^{204}Pb$, $^{87}Sr/^{86}Sr$ and high $^{143}Nd/^{144}Nd$ (Figures 2–7). These peculiar isotopic features have also been reported for gabbros drilled from the eastern wall of the Atlantis II Fracture Zone [*Kempton et al.*, 1991; *Holm*, 2002], which exhibit even lower $^{206}Pb/^{204}Pb$ (down to 16.764) and for peridotites from the Atlantis II transform valley having $^{143}Nd/^{144}Nd$ up to 0.513409 [*Salters and Dick*, 2002]. Similar isotopic attributes also characterize some lavas from the Carlsberg ridge located at 9.8°N near the Owen FZ [*Dupré and Allègre*, 1983; *Mahoney et al.*, 1989]. On the SWIR, this ultra-depleted and homogeneous signature occurs over ~400 km. The two other sections of zone B are more radiogenic in Pb, displaying higher $^{206}Pb/^{204}Pb$, $^{208}Pb/^{204}Pb$ and $^{207}Pb/^{204}Pb$, and lower $^{143}Nd/^{144}Nd$ than section B1 (Figures 3–6). While these sections form two distinct arrays in $^{208}Pb/^{204}Pb$ versus $^{206}Pb/^{204}Pb$, they form a single array in $^{207}Pb/^{204}Pb$ versus $^{206}Pb/^{204}Pb$ (Figure 4). These lavas are also characterized by higher $^{207}Pb/^{204}Pb$ for a given $^{206}Pb/^{204}Pb$ than most of the lavas located to the east of the Melville FZ (Figure 4a). Consideration of $^{87}Sr/^{86}Sr$ as a function of $^{208}Pb/^{204}Pb$, shows that most lavas from section B2 display lower $^{87}Sr/^{86}Sr$ than those from section B3 (Figure 6). In $^{143}Nd/^{144}Nd$ versus $^{87}Sr/^{86}Sr$, samples from sections B2 and B3 fall within the broad negative correlation defined by lavas from zone A (Figure 7).

[16] Within zone C, defined as extending from the Gallieni FZ to Discovery II FZ, two isotopic domains (C1–C2) are clearly identified (Figures 1b–3). A third domain (C3) may exist, but is represented by only one lava from *Hamelin and Allègre* [1985]. Each group (C1–C2) roughly defines a linear array in $^{208}Pb/^{204}Pb$ versus $^{206}Pb/^{204}Pb$, with the section C2 generally having substantially higher $^{208}Pb/^{204}Pb$ for a given $^{206}Pb/^{204}Pb$ than most samples from the area studied (Figure 3) [*Mahoney et al.*, 1992]. For a given $^{208}Pb/^{204}Pb$, samples from the section C1 have higher $^{143}Nd/^{144}Nd$, but similar $^{87}Sr/^{86}Sr$ compared to those from the section C2 and those further to the east (Figure 5).

[17] Within zone D, defined as extending from the Discovery FZ complex to the Prince Edward FZ, four isotopic domains are identified (D1–D4) (Figures 1b–2). All samples from the group D1, bounded by the Discovery FZ complex, display north/central Atlantic or Pacific affinity in Pb and Nd isotopes [*Mahoney et al.*, 1992, Figures 2a–3]. Samples from section D1 have the highest $^{143}Nd/^{144}Nd$, the lowest $^{87}Sr/^{86}Sr$ and $\Delta 8/4$ reported to date for the whole SWIR (Figure 2). Our new sampling for the 39–41°E section, extending from the Eric Simpson to the Discovery FZs, offers new insights into the definition of the remarkable isotopic anomaly previously reported by *Mahoney et al.* [1992]. Samples from this section have been shown to be exceptional in possessing very low $^{206}Pb/^{204}Pb$ (16.877–17.449), $^{143}Nd/^{144}Nd$ (0.5124–0.5128), $^{176}Hf/^{177}Hf$ (0.282768) and high $^{87}Sr/^{86}Sr$ (0.7040–0.7049), $^{207}Pb/^{204}Pb$ (15.414–15.505), $^{208}Pb/^{204}Pb$ (37.245–37.706), $^{187}Os/^{188}Os$ (0.3349) relative to other Indian MORB, but have a typical N-MORB value of $^{3}He/^{4}He$ (7.53) [*Dupré and Allègre*, 1983; *Mahoney et al.*, 1989, 1992; *Chauvel and Blichert-Toft*, 2001; *Escrig et al.*, 2004]. This combination of values is unique to date among oceanic island, seamount and ridge basalts worldwide. Due to their extreme Indian Ocean isotope attributes (Figures 8 and 9), lavas from this section have been considered to provide one of the best examples to date of the component responsible for the isotopic difference between most Indian MORB and their Pacific/north Atlantic counterparts [*Mahoney et al.*, 1992]. Another example of this extreme Indian Ocean anomaly is in lavas from the Aphanasy-Nikitin Rise in the eastern Indian Ocean (Figures 8 and 9), which possibly represent the late Cretaceous product of the Crozet hot spot [*Mahoney et al.*, 1996]. However, this signature does not show any clear affinity with recent products from the Crozet hot spot, and has thus been ascribed either to a temporal change of its isotopic composition or to the presence of continental material in the source of the Crozet plume [*Mahoney et al.*, 1996]. These two unradiogenic $^{206}Pb/^{204}Pb$ signatures are confined to restricted geographic regions of the Indian Ocean.

[18] Our data for the 39–41°E section extend the previously described isotopic ranges to the lowest $^{206}Pb/^{204}Pb$ value (down to 16.58) yet found among oceanic mantle derived rocks (e.g., SWDR13). More importantly, our new sampling shows that the 39–41°E section includes two discrete isotopic domains, identified as D2 and D3 in the figures. The most prominent isotopic anomaly itself (D3) is almost entirely restricted to the segment adjacent to Eric Simpson FZ, where $\Delta 8/4$ are as high as 120 (Figure 2). This anomaly is distinct and does not follow the general trend

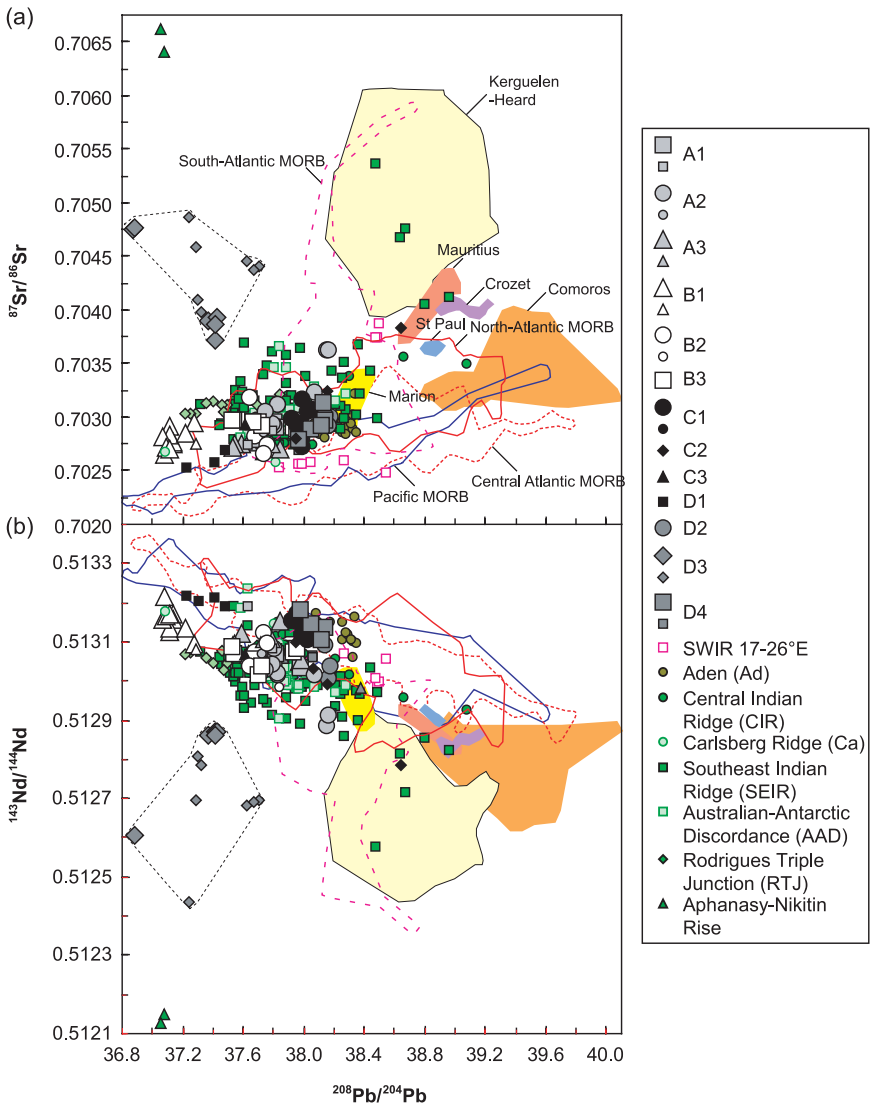

Figure 8. SWIR lavas (a) $^{87}Sr/^{86}Sr$ and (b) $^{143}Nd/^{144}Nd$ against $^{208}Pb/^{204}Pb$ variations compared to north Atlantic, central Atlantic (defined as extending from the Kane to Moore Fracture Zones), south Atlantic and Pacific MORB, Indian Oceanic Island Basalts, and other Indian Ocean spreading centers. Fields have been drawn from data sets including both whole rock and glasses analyses. See Auxiliary Material for references used.[1] Data sources for previous SWIR lavas (small symbols) as in Figure 2.

defined by the main SWIR population (Figures 3–6). The lavas from section D3 are extremely heterogeneous in all isotopic systems, but can themselves be ascribed to two groups (Figure 5). Samples P27 and MD34-D5 from *Mahoney et al.* [1992] are characterized by lower $^{143}Nd/^{144}Nd$, higher $^{87}Sr/^{86}Sr$ for a given $^{208}Pb/^{204}Pb$ and higher $^{208}Pb/^{204}Pb$, $^{207}Pb/^{204}Pb$ for a given $^{206}Pb/^{204}Pb$ than samples from our dredges 10, 13, 14, 15, and 16, and from the dredge P28 from *Mahoney et al.* [1992]. Interestingly, *LeRoex et al.* [1989] also noted the existence of two trends, corresponding to dredges P27 and P28, defined on the basis of trace and major element characteristics. In contrast, samples from the section D2, adjacent to the Discovery FZ, are uniform and are the most radiogenic in $^{206}Pb/^{204}Pb$ (18.407–18.426) of the studied area (Figures 3–7). They are displaced toward lower $^{208}Pb/^{204}Pb$ for a given $^{206}Pb/^{204}Pb$ relative to other sections with the exception of the group B2 (Figures 3b–4b). In all isotopic diagrams, these lavas fall near or slightly overlap the field defined by the Marion hot spot and are similar to lavas from the section 36–39°E (D4) extending from the Eric Simpson FZ to the Prince Edward FZ.

[1]Auxiliary material is available at ftp://ftp.agu.org/apend/gc/2005GC000979.

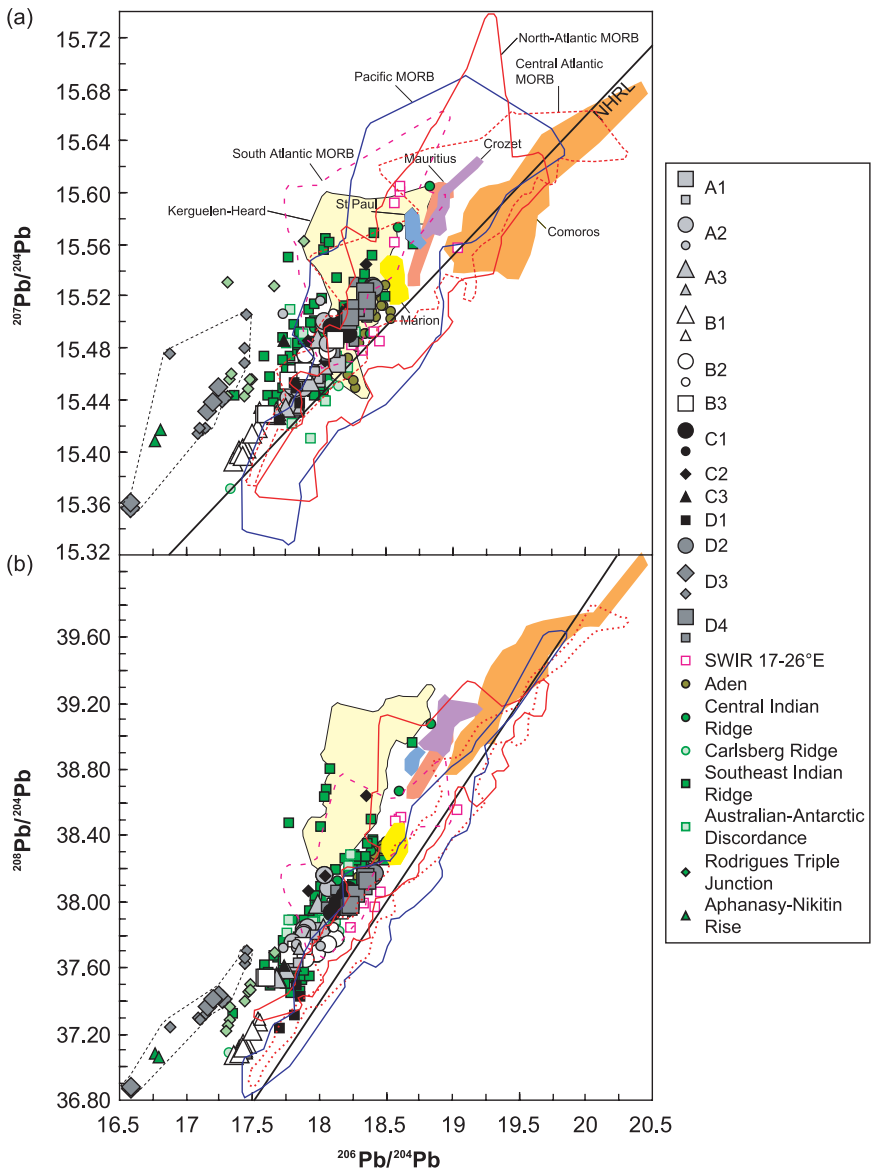

Figure 9. SWIR lavas (a) $^{207}Pb/^{204}Pb$ and (b) $^{208}Pb/^{204}Pb$ against $^{206}Pb/^{204}Pb$ variations compared to north Atlantic, central Atlantic, south Atlantic, and Pacific MORB, Indian Oceanic Island Basalts, and other Indian Ocean spreading centers. Fields have been drawn from data sets including both whole rock and glasses analyses. See Auxiliary Material for references used. NHRL denotes the Northern Hemisphere Reference Line [*Hart*, 1984]. Data sources for previous SWIR lavas (small symbols) as in Figure 2.

3.2. SWIR Lavas Compared to Indian, North Atlantic, and Pacific MORB Arrays

[19] In general, Indian ocean MORB define broadly positive $^{87}Sr/^{86}Sr$ - $^{206}Pb/^{204}Pb$, negative $^{143}Nd/^{144}Nd$ - $^{206}Pb/^{204}Pb$ and positive $^{208}Pb/^{204}Pb$ - ^{206}Pb-^{204}Pb correlations, that are parallel to, but offset from the trend defined by most lavas from the Pacific and Central Atlantic Oceans (Figures 8 and 9). The largest isotopic difference is observed for Indian MORB with $^{206}Pb/^{204}Pb < 18$. In contrast, they overlap with north and south Atlantic MORB (Figures 8 and 9).

[20] In a plot of $^{87}Sr/^{86}Sr$ as a function of $^{208}Pb/^{204}Pb$ (Figure 8a), most lavas from the area studied overlap the north Atlantic and other Indian MORB fields, except those of the RTJ and Aphanasy-Nikitin Rise located to the southern end of the non-seismic 85° East Ridge [*Michard et al.*, 1986;

Price et al., 1986; *Mahoney et al.*, 1996]. The 57–61°E SWIR section (B1) extends the general Indian MORB array to lower $^{87}Sr/^{86}Sr$ and higher $^{143}Nd/^{144}Nd$ for a given $^{208}Pb/^{204}Pb$, as does one sample from the Carlsberg Ridge located near the Owen FZ (Figure 8) [*Dupré and Allègre*, 1983; *Mahoney et al.*, 1989]. The 39–41°E section (D3) forms a vertical trend toward high $^{87}Sr/^{86}Sr$ oblique to the general Indian Ocean population. The same systematic behavior is observed in Nd relative to Pb (Figure 8b), where SWIR samples fall in the general array defined by other Indian ridges trending toward either Kerguelen type Ocean Island Basalt (OIB) or toward Mauritius, St Paul and Crozet OIB. When considered within the same range of $^{208}Pb/^{204}Pb$ (Figure 8b), most samples from the easternmost SWIR, located to the east of the Gallieni Fracture Zone, from the Australian-Antarctic Discordance, from the RTJ and from the Southeast Indian Ridge are characterized by lower $^{143}Nd/^{144}Nd$ than those from the Carlsberg Ridge, Central Indian Ridge, Gulf of Aden and those from the SWIR between 52° and 26°E (with the exception of the groups D3 and C2). All lavas from the Discovery FZ complex (D1), from sections C1 and D4 lie within or closely adjacent to the Pacific/Atlantic arrays.

[21] Overall, the majority of SWIR lavas are consistently higher than Pacific/Central Atlantic MORB in $^{208}Pb/^{204}Pb$ at a given $^{206}Pb/^{204}Pb$ (Figure 9). Most samples located to the west of the Discovery Fracture zone, except those from the section D3, have lower $^{208}Pb/^{204}Pb$ when compared to other Indian MORB with similar $^{206}Pb/^{204}Pb$ values. To the east, some samples from section B2 slightly extend the Indian field toward lower $^{208}Pb/^{204}Pb$ for a given $^{206}Pb/^{204}Pb$. All these samples overlap the north Atlantic, central Atlantic, and Pacific fields.

[22] As would be expected, most of our samples overlap isotope values of other Indian ridges in terms of $^{207}Pb/^{204}Pb$ as a function of $^{206}Pb/^{204}Pb$ (Figure 9). Lavas from the zones B1 and D3 are highly unradiogenic in $^{206}Pb/^{204}Pb$, as are most samples from the RTJ, from the Aphanasy-Nikitin Rise and one sample from the Carlsberg ridge.

4. Discussion

[23] The SWIR represents an isotopic transition between typical Indian Ocean–type compositions to the east and Atlantic like ones west of 26°E [*Mahoney et al.*, 1992]. In the section studied here, east of 35°E, lavas are indeed characterized by the same general features for Sr-Nd-Pb isotopes as Indian MORB. However, in detail, some lavas studied define distinct non-radiogenic end-members in $^{206}Pb/^{204}Pb$ strongly differing in terms of $^{143}Nd/^{144}Nd$, $^{87}Sr/^{86}Sr$, $^{207}Pb/^{204}Pb$ and $^{208}Pb/^{204}Pb$ (groups B1 and D3), which extend the field for Indian MORB (Figures 8 and 9).

[24] Among its other peculiar features, the SWIR is isotopically more heterogeneous over the ~4100 km studied here than other mid-ocean ridges over similar length scales and comparable sampling density. Its degree of heterogeneity (the height of the isotopic shifts in Figure 2) appears to decrease from west to east, and thus to correlate with the regional decrease in crustal thickness, potential mantle temperature and increasing depth [*Francis and Raitt*, 1967; *Minshull and White*, 1996; *Müller et al.*, 1997, 1999, 2000; *Cannat et al.*, 1999; *Meyzen et al.*, 2003]. Hence most of the isotopic heterogeneity appears to be confined to the west of the Indomed FZ. In this section, we will begin by discussion of the boundary between the easternmost SWIR and the Rodrigues Triple Junction. We will then discuss the large and small scale isotopic variations of SWIR lavas. Finally, we investigate the possible origin of the low $^{206}Pb/^{204}Pb$ component present in the group D3 and its role in the genesis of the distinctive Indian mantle signature.

4.1. Regional Isotopic Heterogeneity From Large- to Small-Scale Domains Along the SWIR and in the Vicinity of the SWIR

4.1.1. A Boundary Between the Rodrigues Triple Junction and the Easternmost Southwest Indian Ridge

[25] The Rodrigues Triple Junction (RTJ, 25°33′S, 70°E), which has been stable for about ~40 Myr, connects the Southeast Indian Ridge (SEIR), the Central Indian Ridge (CIR) and the SWIR [*Sclater et al.*, 1981; *Patriat and Segouffin*, 1988]. Its northeastward migration during the last ~74 Myr has produced a lengthening of the SWIR [*Royer et al.*, 1988]. Presently, it is moving at 20 mm yr^{-1}, almost three times the half spreading rate of the eastern SWIR [*Tapscott et al.*, 1980; *Patriat et al.*, 1997]. Near the junction, there is no evidence from gravity data for focused upwelling beneath the SWIR limb; spreading is thus primarily amagmatic [*West et al.*, 1995; *Rommevaux-Jestin et al.*, 1997]. The mantle flow pattern in this region has

thus been inferred to be principally dominated by upwelling of the two intermediate SEIR and CIR spreading ridges, leading to sampling of their lateral down flow residual mantle by the slow SWIR branch [*Mitchell*, 1991; *West et al.*, 1995]. However, this view has been questioned by recent numerical 3D modeling of mantle flow and temperature structure at the RTJ, which shows that the SWIR mantle flow has a strong component of along-axis velocity directed away from the junction [*Georgen and Lin*, 2002]. This would result in almost no material transfer from the faster to the slower-spreading ridges [*Georgen and Lin*, 2002].

[26] The easternmost SWIR samples are located at a minimum distance of ~78 km from the RTJ and are isotopically distinct from those at the junction in having lower $^{87}Sr/^{86}Sr$, $^{208}Pb/^{204}Pb$ and $^{207}Pb/^{204}Pb$ for a given $^{206}Pb/^{204}Pb$ (Figures 2, 3, 5, and 7). The isotopic discontinuity between lavas from the RTJ and those from the easternmost SWIR was first recognized by *Mahoney et al.* [1989], who attributed it to either (1) isotopically distinct mantle domains whose boundary coincides with the RTJ or (2) a vertically zoned mantle, which is sampled differentially due to contrasts in fertility or as a result of differences in mantle temperature under the ridges.

[27] If the mantle is vertically zoned with blobs of low $^{206}Pb/^{204}Pb$ material present below the site of onset of melting of the SWIR mantle (assuming that melting begins at greater depth beneath the RTJ than the SWIR), a correlation between the mean axial depth and Pb isotopes for lavas from the SWIR and RTJ would be expected. Although not shown, there is no such isotopic correlation. The isotopic discontinuity observed between the easternmost SWIR and the RTJ appears therefore to be the surface expression of a rather abrupt boundary between different mantle domains, supporting the numerical modeling of *Georgen and Lin* [2002]. A similar isotopic boundary should exist between the CIR and the RTJ, as mantle flow beneath the CIR is predicted to be directed away from the junction [*Georgen and Lin*, 2002]. However, the northward extent of the RTJ domain along the CIR cannot be precisely determined due to a lack of geochemical data on the CIR between 21.5° and 24.9°S. Discussion on whether or not mantle flow patterns presently observed at the RTJ have persisted through time and space is rather speculative and would require further off-axis sampling of the fossil RTJ.

4.1.2. Isotopic Provinces in the SWIR Mantle

4.1.2.1. Large-Scale Isotopic Variations

[28] To a first approximation, the Pb isotopes show some evidence for a subtle, but irregular regional variation in source composition (increase in Δ8/4 going from west to east, broadly correlated with a decrease in $^{206}Pb/^{204}Pb$, Figure 2), which may reflect some form of large-scale mantle flow and mixing. This compositional gradient has previously been proposed to arise from the dispersion of the low $^{206}Pb/^{204}Pb$ component sampled by the section D3 by Marion, Kerguelen and Crozet plumes during the breakup of Gondwanaland. This component was then carried by shallow level convection following the northerly to northeasterly spreading direction of the Indian plate during the period of superfast spreading from 80 to 43 Ma [*Mahoney et al.*, 1992]. However, this model is not supported by our isotopic data. Toward the east, the baseline $^{87}Sr/^{86}Sr$ broadly decreases to ~65°E, instead of increasing as would be expected (Figure 2). The longitudinal $^{143}Nd/^{144}Nd$ profile does not show any clear decreasing gradient from west to east along the area studied (Figure 2).

[29] As mentioned above, the degree of source heterogeneity seems to decrease from west to east, and thus correlates with the regional decrease in crustal thickness, potential mantle temperature and increasing depth [*Francis and Raitt*, 1967; *Minshull and White*, 1996; *Müller et al.*, 1997, 1999, 2000; *Cannat et al.*, 1999; *Meyzen et al.*, 2003]. Furthermore, the largest isotopic diversity appears to be restricted to the west of the Indomed FZ and is thus not related to the eastward decrease of the full spreading rate (from ~1.6 cm yr^{-1} to ~1.2 cm yr^{-1} [*Chu and Gordon*, 1999]) along the area studied. *Allègre et al.* [1984] argued that isotopic diversity is inversely related to spreading rate, resulting from less effective homogenization of heterogeneities by magmatic processes at slow to ultra slow spreading ridge. Other researchers have questioned this fact as for example low, instead of high variability of $^{3}He/^{4}He$ is observed in SWIR basalts relative to other MORB [e.g., *White et al.*, 1987; *Georgen et al.*, 2003]. Our SWIR data also discounts a relationship with spreading rate. Alternatively, as the greatest isotopic diversity occurs in the vicinity of fracture zones, this may be related to a local transform fault effect, as discussed below.

4.1.2.2. Role of Transform Faults

[30] The studied section of the SWIR is characterized by the presence of transform faults, simple strike-slip translational plate boundaries, which offset the ridge axis laterally in the direction of plate motion. These tectonic lithospheric features are usually associated with a decrease in crustal thickness and an increase in axial depth, reflecting a locally colder mantle temperature due to conductive heat loss through the adjacent older lithosphere [*Langmuir and Bender*, 1984; *Shen and Forsyth*, 1995]. At transform-ridge intersections, where low degrees of melting are predicted, veins enriched in volatile, large-ion lithophile elements, and radiogenic Pb and Sr would be expected to contribute in greater proportion to the liquid relative to the depleted matrix [*Langmuir and Bender*, 1984]. Such gradients toward more enriched signatures are only found in the shallowest part of the ridge (Figure 2), in the vicinity of the Indomed Fracture Zone (group C2) and the Eric Simpson Fracture Zone (group D3), where the regional mantle temperature is expected to be hottest. To a first approximation, this observation is consistent with the fact that such an effect would be expected to be enhanced when the regional mantle temperature is hot rather than cold. However, detailed examination shows that the maxima in $\Delta 8/4$ and $^{87}Sr/^{86}Sr$ for the group D3 do not occur adjacent to the transform, suggesting that these maxima may not be controlled by a transform fault effect. In addition, previous geochemical studies of the major and trace element compositions of MORB over this area have emphasized the absence of a transform fault effect [*LeRoex et al.*, 1989].

[31] Finally, at least to the east of the Indomed Fracture Zone, steps in isotopic compositions in Pb and to a lesser extent in Nd between different isotopic domains coincide with the locations of long-offset (>90 km) transform faults (e.g., Gallieni, Atlantis II and Melville FZs), which indicate that there is no continuity in mantle flow beneath these fracture zones (Figure 2). Although transform faults have been shown to correspond in some areas with isotopic boundaries (e.g., Hayes Fracture Zone, Kane Fracture zone and Southern Chile Ridge [*Machado et al.*, 1982; *Smith et al.*, 1998; *Sturm et al.*, 1999]), it is far from being a general feature along the worldwide mid-ocean ridge system.

4.1.2.3. Small-Scale Isotopic Domains

[32] Overall, given the present sampling, the extents of small-scale isotopic domains do not coincide with bathymetric segmentation (Figures 1b–2). In other words, the trends (Figures 3–7) defined by the groups are not generally geographically restricted to one segment, and continue across segment boundaries, with the exception of the group B2. The presence of these small-scale isotopic domains does not appear to be a characteristic inherent to regions of ultra-slow spreading rate. Such domains spanning a few degrees of longitude (less than 1° to 5°) have also been found along the East Pacific Rise and the Southern Chile Ridge [*White et al.*, 1987; *Sturm et al.*, 1999, *Galer et al.*, 1999].

[33] The spatial distribution observed here indicates that the SWIR mantle is heterogeneous at shallow level with respect to Pb, Nd and to a lesser extent, Sr isotopes. The degree of heterogeneity, or at least the sampling of these heterogeneities, appears to diminish from west to east along the ridge. In Pb isotope space, the arrays defined by the most radiogenic sections do not trend toward the same depleted end-member composition and do not converge on the component defined by the 57–61° section, which clearly suggests the existence of different ''depleted'' ambient mantle compositions (Figures 3 and 4). As shown by the fan described by these arrays in $^{208}Pb/^{204}Pb$ versus $^{206}Pb/^{204}Pb$ at high $^{206}Pb/^{204}Pb$ (Figure 3b–4b), different components characterized by distinct $^{208}Pb/^{204}Pb$ are involved in the mixing relationships, and must be present as streaks in the upper mantle, and are not related to flow from mantle plumes such as Crozet to the east of Gallieni FZ. Alternatively, recent in situ Pb-isotope studies of olivine-hosted melt inclusions for OIB reveal extreme $^{207}Pb/^{206}Pb$ – $^{208}Pb/^{206}Pb$ heterogeneity, at the sample scale [*Saal et al.*, 1998], which may arise from a locally heterogeneous source [*Hofmann*, 2003]. The scales of heterogeneities observed along the SWIR may thus reflect distinct scales of homogenization resulting from mixing during the aggregation process of primary liquids and melting process (e.g., volume of melting) rather than the melting of different heterogeneous sources. Shallow level mixing and homogenization processes would dampen much of the source heterogeneity.

[34] Along the SWIR, there is thus no evidence for vigorous, widespread and long-term convection which would have efficiently homogenized the mantle, at least at the scale of present sampling, >~308 km. Future mapping by high precision Pb isotopes of small scale isotopic domains and un-

derstanding of how these domains maintain their integrity should prove useful for understanding the geometry of mantle heterogeneity and mixing process, as well as for the detailed origin of isotopic variations of the upper mantle.

4.2. Origin of the Low $^{206}Pb/^{204}Pb$ Component and Mixing Relationships in the Indian Ocean Mantle

4.2.1. Origin of the Low $^{206}Pb/^{204}Pb$ Component Observed Between 39 and 41°E Section: Recycled Oceanic Components Versus Recycled Continental Components

[35] Lavas from the 39–41°E section, along with those from the Aphanasy-Nikitin Rise are of particular interest as they exhibit by far the strongest typical Indian signatures yet found in the Indian Ocean. These anomalies are highly focused on these two particular regions, but the component is variably distributed throughout the Indian Ocean mantle source (Figures 8 and 9).

[36] Isotopically, the shapes of the fields, and especially the quadrilateral pattern defined by these lavas in $^{143}Nd/^{144}Nd$ and $^{87}Sr/^{86}Sr$ versus $^{208}Pb/^{204}Pb$ require the involvement of more than two end-members (Figure 5). Their isotopic compositions indicate a weaker contribution of melts from a normal MORB mantle beneath this part of the SWIR, and hence a higher contribution of melts arising from a low $^{206}Pb/^{204}Pb$ component. Below we discuss several possible origins for the low $^{206}Pb/^{204}Pb$ component of the 39–41°E lavas.

4.2.1.1. Hot Spot

[37] Although lavas from the group D3 geographically fall in the southern extension of the Madagascar Rise, which is the presumed post–80 Ma trace of the Marion hot spot on the African plate (Figures 1 and 2) [*Storey et al.*, 1995], they do not trend toward the Marion hot spot field, as clearly emphasized by their $^{207}Pb/^{204}Pb$ - $^{206}Pb/^{204}Pb$ variations (Figure 3a). In addition, on a world-wide scale, no present-day hot spots exhibit the isotopic heterogeneity that would be required, not even the EM1 type Ocean Island Basalts from Walvis Ridge, Kerguelen and Pitcairn islands (Figures 10 and 11). There is also no evidence that the low $^{206}Pb/^{204}Pb$ component is an intrinsic feature of the present-day Marion hot spot, as would be expected by the presence of the two types of lavas within the anomaly. However, paradoxically, isotopic compositions of lavas from both sections (groups D2 and D4) adjacent to the group D3 can be accounted for by a mixture of Marion hot spot and the depleted end-member expressed by Discovery lavas (group D1) (Figures 3, 5, and 7). Lavas from the group D2 fall very close to or overlap the field defined by the Marion hot spot. Those from the section D4 fall along possible mixing curves between Marion hot spot and Discovery lavas (Figures 3, 5, and 7). This binary model is further supported by a Principal Component Analysis using the Pb isotope ratios (relative to ^{206}Pb) where 98.4 % of the variance is confined to the first principal axis. Even the scatter observed in $^{143}Nd/^{144}Nd$ and $^{87}Sr/^{86}Sr$ versus $^{208}Pb/^{204}Pb$ is consistent, provided that a certain degree of heterogeneity is allowed in the two end-members. The calculated contribution of Marion hot spot material ranges from 10 to 50% consistent with a contribution of ~40% proposed by *Mahoney et al.* [1992] in the source of lavas from the section D4. However, the complex, irregular and asymmetric dispersion of enriched mantle associated with the Marion plume along the ridge axis appears to be inconsistent with radial mixing models such as those established for faster spreading ridges [e.g., *Schilling et al.* 1999].

4.2.1.2. Sediment

[38] Sedimentary material in the oceanic mantle could result from recycling via subduction of oceanic lithosphere [e.g., *Hofmann and White*, 1982; *Weaver*, 1991]. The composition of a deep sea sediment column is a function of its lithological constituents which are a function of the different detrital sources and of the sedimentation rate [*Plank and Langmuir*, 1998]. Many sediments have low $^{238}U/^{204}Pb$ ratios (2–6) meaning that old sediment might be characterized by low $^{206}Pb/^{204}Pb$ compared to modern values [e.g., *Ben Othman et al.*, 1989; *Rehkämper and Hofmann*, 1997].

[39] Considering the ''erosion mix'' curves [*Kramers and Tolstikhin*, 1997; *Nägler and Kramers*, 1998], which represent the modeled Nd-Pb isotopic evolution of terrestrial sediment that has been subducted into the mantle throughout Earth's history, it may be assessed whether the Pb-Nd isotopic characteristics of group D3 can be of sedimentary origin or not. From the ''erosion mix Pb curve,'' the μ required to produce lavas from the group D3 via the ^{235}U and ^{238}U decay equations has been calculated. For the whole group D3, the solutions converge at ~3.55 Ga. The group D3 can

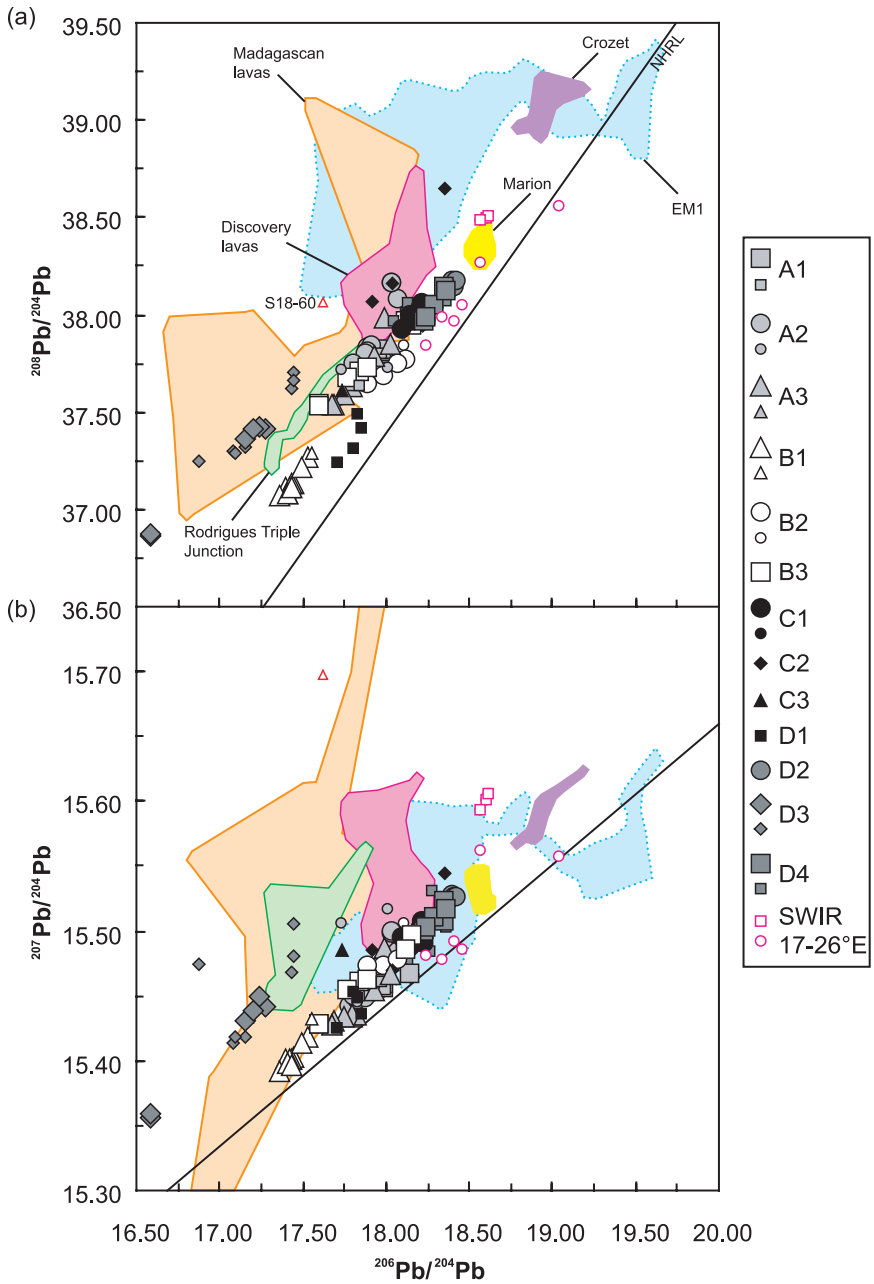

Figure 10. SWIR lavas (a) $^{208}Pb/^{204}Pb$ and (b) $^{207}Pb/^{204}Pb$ against $^{206}Pb/^{204}Pb$ variations compared to Discovery lavas [*Douglass et al.*, 1999], sample S18-60 from the southern mid-Atlantic ridge near the Bouvet Triple junction [*Kamenetsky et al.*, 2001], Madagascan lavas [*Mahoney et al.*, 1991; *Storey et al.*, 1997], and global isotopic end-member EM1 (See Auxiliary Material for references used). Data sources for previous SWIR lavas (small symbols) as in Figure 2.

be derived from "erosion mix" with initial $^{206}Pb/^{204}Pb$, $^{207}Pb/^{204}Pb$ and $^{208}Pb/^{204}Pb$ values of 12.03, 13.83 and 31.67 with a μ of 6.92 and a $^{232}Th/^{238}U$ (κ) of 4.27 at 3.55 Ga. All these μ and κ values are well within the range of those observed for sediment. However, the initial value obtained for $^{143}Nd/^{144}Nd$ of 0.5125 at ~3.55 Ga, is very close to the present-day average composition of the group D3 (0.5127), requiring an unrealistic low $^{147}Sm/^{144}Nd$ (0.010) for the sediment component (0.10–0.17, [*Strake et al.*, 2003]). Therefore the Nd-Pb systematics cannot be accounted for by the presence of sediment in the source, given current constraints on such modeling. Further evidence

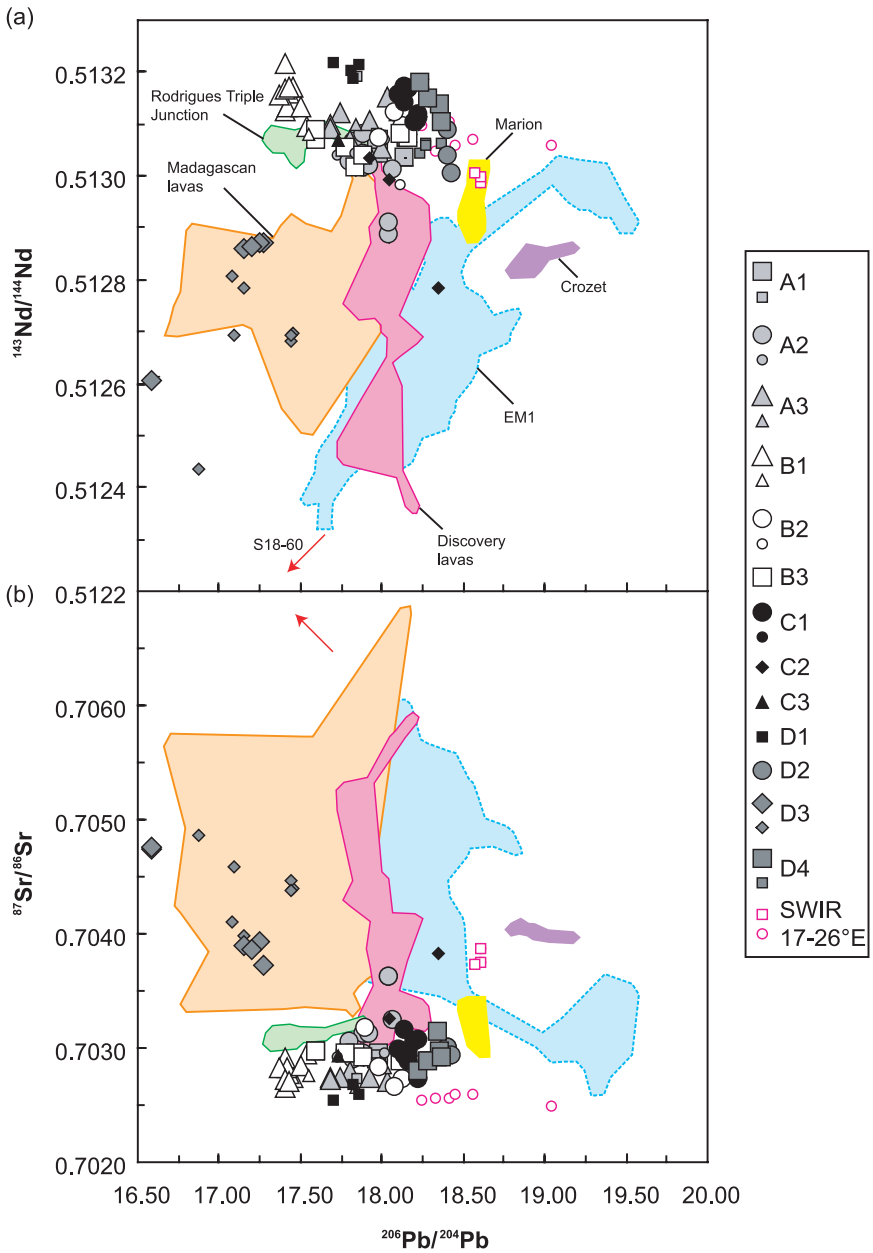

Figure 11. SWIR lavas (a) $^{143}Nd/^{144}Nd$ and (b) $^{87}Sr/^{86}Sr$ against $^{206}Pb/^{204}Pb$ variations compared to Discovery lavas [*Douglass et al.*, 1999], sample S18-60 from the southern mid-Atlantic ridge near the Bouvet Triple junction [*Kamenetsky et al.*, 2001], Madagascan lavas [*Mahoney et al.*, 1991; *Storey et al.*, 1997], and global isotopic end-member EM1 (See Auxiliary Material for references used). Data sources for previous SWIR lavas (small symbols) as in Figure 2.

against sediment as a component of D3 lavas is provided by their relatively variable $^{207}Pb/^{204}Pb$ and relatively constant $^{208}Pb/^{204}Pb$ (Figure 3) and hence variable U/Pb and constant Th/Pb parent/daughter ratios, as no group of sediments has variable U/Pb and constant Th/Pb parent daughter ratios [*Strake et al.*, 2003; *Ben Othman et al.* 1989]. These characteristics can also not arise from subduction processing, as sediment melting and fluid sediment release processes affect the Th/Pb and U/Pb of sediment to a similar degree, leading to preservation of the U/Pb and Th/Pb features [*Strake et al.*, 2003]. Therefore recycled oceanic components, sediment ± oceanic crust can also be discarded as source components for the group D3. Similar conclusions have been recently reported at

Table 3. Melting Model Results[a]

	Partition Coefficient					Garrett Lavas		Aleutian Lavas		
	Ol	Cpx	Opx	Sp	Bulk D	$(CL)_8$	C_0	$(CL)_6$	C_0	Cwedge
Na	-	-	-	-	0.030	2.70	0.3	-	-	-
Pb	0.0076	0.020	0.0013	-	0.018	0.42	0.041	4.82	0.70	0.024
Th	0.000014	0.021	0.0032	0.001	0.005	0.06	0.006	1.44	0.21	0.0041
U	0.000059	0.018	0.0047	0.001	0.005	0.09	0.008	0.72	0.10	0.0020
Zr	0.00015	0.18	0.027	0.05	0.043	-	-	78.72	12.93	-
$^{206}Pb/^{204}Pb$							17.754			18.854
$^{207}Pb/^{204}Pb$							15.374			15.568
$^{208}Pb/^{204}Pb$							37.131			38.396

[a] Pb, U, and Th concentrations are in ppm. The isotopic average composition of the depleted Pacific is from *Wendt et al.* [1999]. The isotopic average composition of the wedge source is from *Miller et al.* [1994], *George et al.* [2003, 2004], and *Class et al.* [1999]. Fractionation corrected concentration at MgO = 6% and MgO = 8% are determined from regression from the Aleutian arc and Garrett transform lavas [*Class et al.*, 1999; *Wendt et al.*, 1999; *Miller et al.*, 1994; *George et al.*, 2003, 2004] following the approach developed by *Klein and Langmuir* [1987], *Plank and Langmuir* [1988], and *Langmuir et al.* [1992]. Data are filtered out between 5 and 8.5% MgO for normalized oxides. The initial mode is from *Kinzler and Grove* [1992]. The partition coefficients are from *McDade et al.* [2003], *McKenzie and O'Nions* [1991], *Dunn and Sen* [1994], and *Niu et al.* [1999].

the basin wide scale by several investigators [*Kempton et al.*, 2002; *Escrig et al.*, 2004].

4.2.1.3. Subduction Modified Subarc Mantle

[40] An alternative origin for the 39–41° section (group D3) is that it represents subduction modified subarc mantle, which has undergone metasomatism and melting at the subduction zone before being recycled into the deep mantle through viscous coupling to the down going slab. Recently, on the basis of Hf-Nd systematics, *Kempton et al.* [2002] have argued that the distinct nature of Indian MORB may originate from the presence of a substantial proportion of material arising from subduction modified mantle embedded in the shallow asthenosphere. However, this model has not been constrained for Pb isotopes. A first step to model the Pb isotope composition of subduction modified subarc mantle is to find an oceanic arc which does not exhibit an Indian-like signature. Most (if not all) oceanic arc lavas currently produced within the western Pacific Ocean arise from Indian type mantle [*Hergt and Hawkesworth*, 1994; *Shinjo et al.*, 2000]. Among other arcs, the second and central Aleutian arcs meet these requirements. In order to determine the U, Pb and Th contents of the residual mantle wedge, we have assumed that the Aleutian average in $Zr_{6.0}$ (Zr normalized to 6% MgO [*Plank and Langmuir*, 1988]) represents a 14% accumulated fractional melt assuming that (1) negligible amounts of Zr are added during subduction and (2) the Zr content of the mantle wedge is equal to that of the depleted Pacific mantle. The U-Th-Pb contents of the residual wedge can then be estimated from the average composition of these lavas as we know the extent of melting and the partition coefficients of U, Th and Pb. The average isotope composition of these arc lavas can then be corrected back in time. A broadly similar approach is used to age-correct the average isotope composition of the depleted Pacific mantle taken as being represented by Garrett transform lavas. U, Th and Pb contents are inversely calculated assuming that the average in $Na_{8.0}$ of lavas from the Garrett transform fault [*Wendt et al.*, 1999] represents a 9% accumulated fractional melt. The parameters and details of the calculations are given in Table 3. Knowing all these parameters, we can then determine the present-day isotopic composition using the ^{235}U, ^{238}U and ^{232}Th decay equations of an old mixture between these components. Both Indian and Atlantic Oceans overly a mantle cell, which has contained all continents for at least 400 Myr, meaning that it has been circled and crossed by subduction zones [*Collins*, 2003]. We thus have assumed a mixture occurring 400 Myr ago between a depleted Pacific mantle and a subarc wedge. The attributes of the composition of the present-day mixture cannot represent a plausible end-member for the group D3 (see Figure 12). Similar conclusions are valid for more ancient components as old subduction modified subarc mantle does not yield high enough $^{207}Pb/^{204}Pb$ and $^{208}Pb/^{204}Pb$ to explain the group D3 (Figure 12a). Nevertheless, the presence of recycled metasomatic-mantle components merits further investigation, as dewatering slab processes have been a major process throughout Earth history.

4.2.1.4. Sublithospheric Continental Mantle

[41] The observation of isotopic similarities between cretaceous alkali lavas from Madagascar

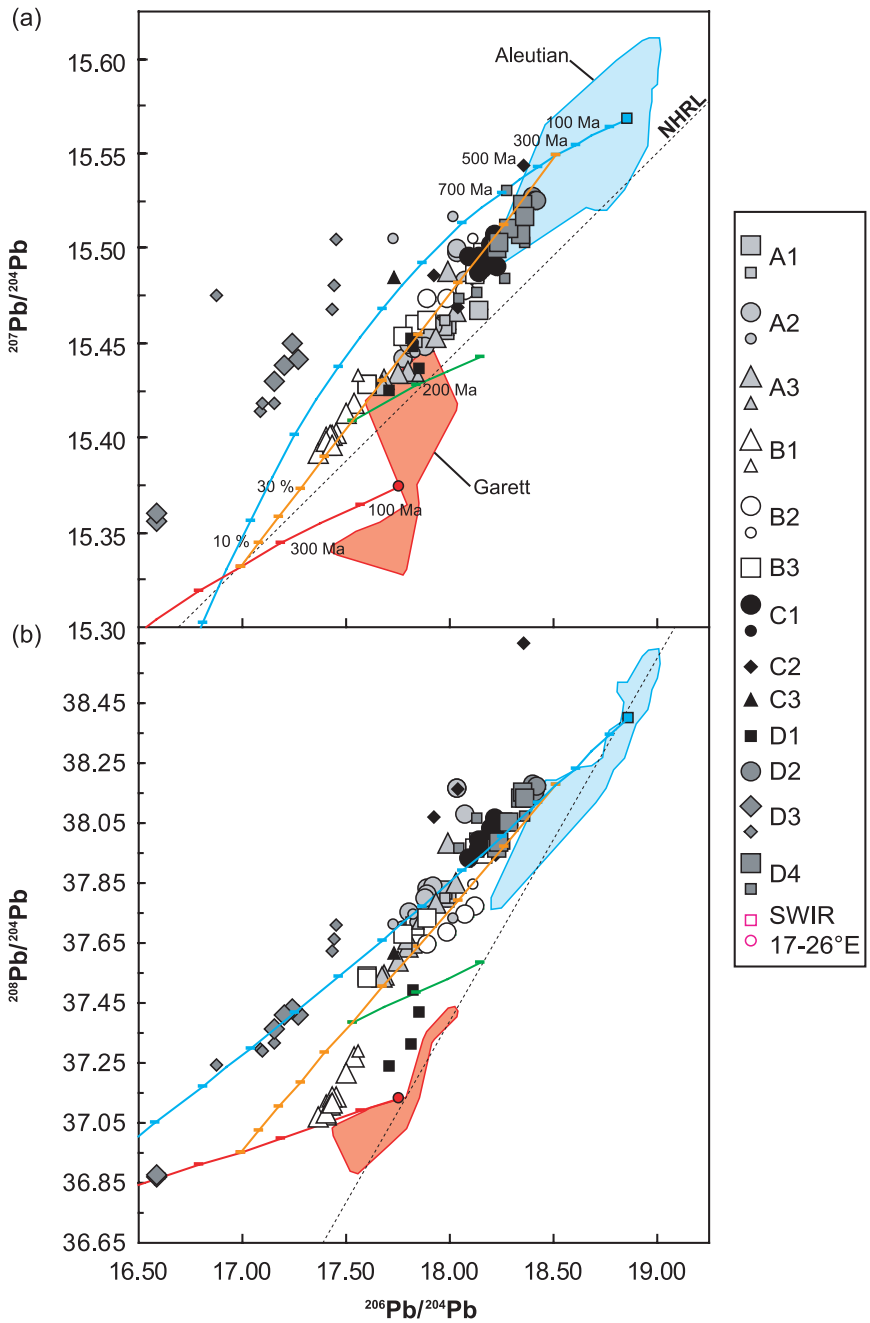

Figure 12. Diagrams of (a) $^{207}Pb/^{204}Pb$ and (b) $^{208}Pb/^{204}Pb$ versus $^{206}Pb/^{204}Pb$ which demonstrate the mixing systematics of the proposed mantle wedge contamination model. The isotopic compositions of SWIR lavas, as well as fields for Aleutians lavas [*Miller et al.*, 1994; *George et al.*, 2003, 2004; *Class et al.*, 1999] and Garrett transform lavas [*Wendt et al.*, 1999], are shown for comparison. The blue and red curves represent the initial compositions of the mantle wedge and of the depleted Pacific mantle, respectively, recalculated by age correction every 200 Myr. The orange curve is the mixture of these two end-members at 400 Ma with steps of 10%. The green curve is the isotopic composition of the mixture from 400 Ma to present-day, graduated by 200 Myr.

and lavas from the 39–41°E section (e.g., low $^{206}Pb/^{204}Pb$, high $^{208}Pb/^{204}Pb$, high $^{207}Pb/^{204}Pb$, low $^{143}Nd/^{144}Nd$ and high $^{87}Sr/^{86}Sr$) led *Mahoney et al.* [1992] to suggest that they tap the same component, the Madagascan continental lithosphere (Figures 10 and 11). A portion of Madagascan lithosphere may have been thermally eroded from Indo-Madagascar by the action of the Marion hot spot and incorporated within the shallow asthenosphere just before the breakaway of

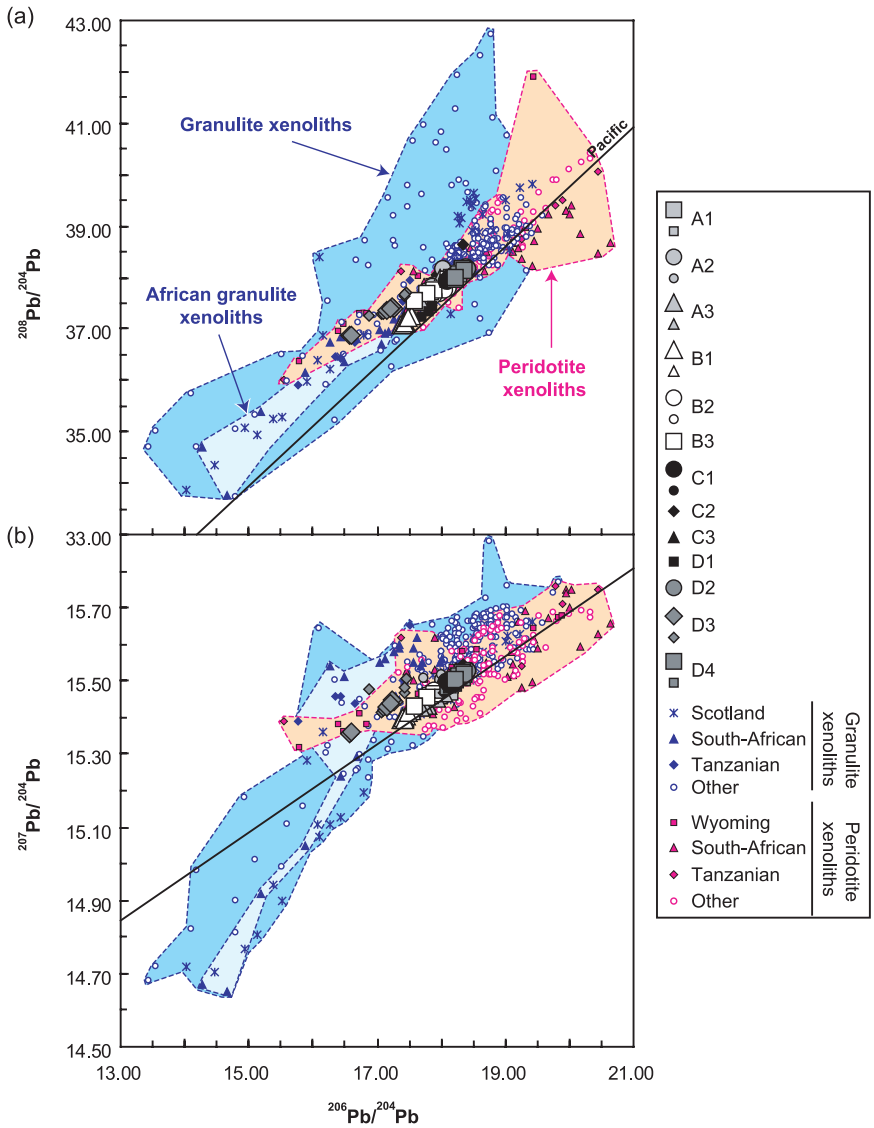

Figure 13. SWIR lavas (a) $^{208}Pb/^{204}Pb$ and (b) $^{207}Pb/^{204}Pb$ against $^{206}Pb/^{204}Pb$ variations compared to granulite, peridotite xenoliths, and Pacific array. See Auxiliary Material for references used. The Pacific array has been determined by a regression line through the data from Figures 8 and 9. Data sources for previous SWIR lavas (small symbols) as in Figure 2.

Madagascar from greater India [*Mahoney et al.*, 1992]. Such contamination models supported by plume activity have been invoked to account for the distinctive signature of MORBs from the Indian and South Atlantic Oceans [*Douglass et al.*, 1999; *Mahoney et al.*, 1992]. In turn, some lavas from the Discovery anomaly and from the southernmost segment of the mid-Atlantic Ridge [*Kamenetsky et al.*, 2001], converge toward a low $^{206}Pb/^{204}Pb$, $^{143}Nd/^{144}Nd$ and high $^{87}Sr/^{86}Sr$, $^{207}Pb/^{204}Pb$, $^{208}Pb/^{204}Pb$ component, but are characterized by much higher $^{206}Pb/^{204}Pb$ than that of the group D3 (Figures 10 and 11).

[42] The attractiveness of the sublithospheric continental mantle as a primary source for the 39–41°E section and for Indian MORB in general, is its potential to act as an ancient, stagnant and highly heterogeneous reservoir due to metasomatic enrichment. However, the hypothesis that some MORB and OIB could be derived from cool, refractory sublithospheric continental mantle has been increasingly questioned [e.g., *McKenzie and Bickle*, 1988; *Arndt and Christensen*, 1992; *Arndt et al.*, 1993; *Rëkhamper and Hofmann*, 1997; *Kempton et al.*, 2002; *Escrig et al.*, 2004]. Post-Archean continental mantle lithosphere is the most

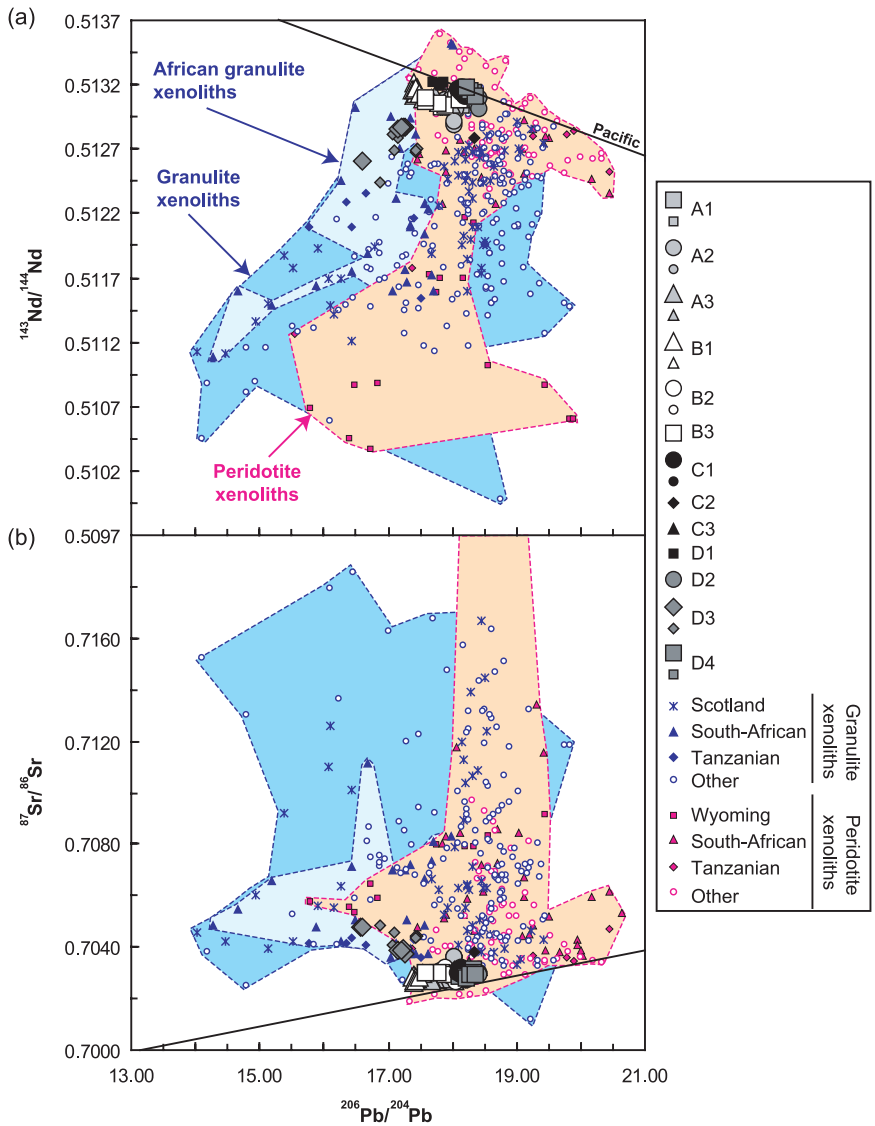

Figure 14. SWIR lavas (a) $^{143}Nd/^{144}Nd$ and (b) $^{87}Sr/^{86}Sr$ against $^{206}Pb/^{204}Pb$ variations compared to granulite, peridotite xenoliths, and Pacific array. See Auxiliary Material for references used. Data sources for previous SWIR lavas (small symbols) as in Figure 2.

likely lithospheric material to be removed by mantle processes because of its inherently higher density and weaker nature [*Pearson and Nowell*, 2002]. However, post-Archean peridotite xenoliths from southern Africa do not possess the very low $^{206}Pb/^{204}Pb$ signature (<16.5) required to be a source component for lavas from the 39–41°E SWIR section (Figures 13 and 14) [*Kramers*, 1977; *Kramers et al.*, 1983; *Hawkesworth et al.*, 1990]. On a worldwide scale, even among the xenoliths assumed to represent Archean sublithospheric mantle, only two suites of xenoliths from Wyoming [*Carlson and Irving*, 1994] and Tanzania [*Cohen et al.*, 1984] display low enough $^{206}Pb/^{204}Pb$ (Figures 13 and 14). Such signatures are extremely rare within the sublithospheric continental mantle (Figures 13 and 14). Finally, the high $^{187}Os/^{188}Os$ (0.3349) of one of the most unradiogenic $^{206}Pb/^{204}Pb$ sample (MD34-D5, Figure 3) of the section D3 discounts this material as being a source component for this group, as mantle xenoliths are typically characterized by subchondritic Os isotopes (on average 0.1214 ± 0.0078 [*Escrig et al.*, 2004]).

4.2.1.5. Lower Crust

[43] It is possible that recycled material characterized by low μ from the lower crust is a component

in the source of the 39–41°E section. The dispersion in $^{207}Pb/^{204}Pb$ at a given $^{206}Pb/^{204}Pb$ observed for group D3 requires this material to be old, in light of the rapid decay of ^{235}U. "Delamination" of lower continental crust represents an alternative mechanism for recycling continental material into the convective upper mantle [e.g., *Arndt and Goldstein*, 1989; *Turcotte*, 1989; *Kay and Kay*, 1993]. "Delamination" sensu stricto results in a transformation of the mafic lower crust into a high-density mineral assemblage, due to thickening and cooling processes, which then sinks into the underlying lower density mantle [*Arndt and Goldstein*, 1989; *Turcotte*, 1989; *Kay and Kay*, 1993]. This process is favored in environments such as arcs, volcanic rifted margins and continental areas which are experiencing extension or removal of the underlying mantle [*Jull and Kelemen*, 2001]. On the basis of modeling of Nd and Th-U-Pb system for the upper mantle, such a recycling process appears to have been important after 2–1.6 Ga [*Nägler and Kramers*, 1998].

[44] Whether or not lower crust is a suitable component for group D3 can be assessed from the isotopic composition of lower crustal material which is brought to the surface as garnet granulite xenoliths (Figures 13 and 14). The isotopic compositions of such xenoliths, which come from depths between 25 and 45 km, vary greatly from one region to another depending on the nature of their protholith [e.g., *Rudnick and Goldstein*, 1990; *Rudnick and Fountain*, 1995]. At a worldwide scale, most granulite xenoliths are characterized by higher $^{207}Pb/^{204}Pb$ and $^{208}Pb/^{204}Pb$, for a given $^{206}Pb/^{204}Pb$ (Figure 13) and higher $^{87}Sr/^{86}Sr$ values and lower $^{143}Nd/^{144}Nd$ (Figure 14) compared to Pacific MORB. Nevertheless, a few sites (Scotland, southern Africa, and Tanzania) are characterized by extremely low μ values (Figures 13 and 14). Their low μ signature is related to Archean or Proterozoic metamorphic U and Th loss from the lower crust during orogenic events, either by partial melting or fluid flushing [*Downes et al.*, 2001]. Among these granulite xenoliths, those from the kimberlite craton-margin of southern Africa [*Huang et al.*, 1995] which are ~1.1 Ga [*Schmitz and Bowring*, 2000], have the required composition to be an end-member for group D3 (Figures 13 and 14). Remnants of lower continental crust from craton margin lithosphere might have been stripped off and incorporated into the asthenosphere either during the breakup of Gondwana [*Escrig et al.*, 2004] or during the convergence of continental plates. Similar scenarios have been proposed by several investigators to account for the features of the DUPAL basalts at the basin-wide scale [*Arndt and Goldstein*, 1989; *Escrig et al.*, 2004; *Hanan et al.*, 2004], suggesting the widespread incorporation of material from the Gondwanaland lower crust in the shallow asthenosphere during breakup of the supercontinent. Isotopically the lower crust would therefore appear to be the most reasonable petrological component responsible for the isotopic characteristics of the group D3 lavas.

4.2.1.6. Mode of Incorporation

[45] From a geodynamic perspective, the presence of a crustal component raises a number of important questions. For example, if lower crustal remnants have been thermally eroded by the Marion plume just before the breakaway of Madagascar from greater Indian and incorporated within the upper mantle, this would leave little time for this material to be dispersed throughout the present-day Indian source. In addition, during continental breakup, remnants of lower crust are expected to be pushed away from the ridge axis due to the perpendicular direction of the flow lines. This implies that remnants of lower crust during continental breakup must have been incorporated at depth where flow away from the axis was minimal, which appears an unlikely mechanism during continental breakup. Alternatively, this material may have been detached during ancient continental collision/subduction and incorporated into the upper mantle. This would require either ancient storage of this material into a discontinuity layer or ancient mixing of lower crustal material into the Indian mantle source. A recent isotopic study of Tethyan basalts and gabbros has revealed that Indian Ocean type mantle was widespread beneath the Neotethys in the Jurassic and Early Cretaceous and present beneath at least parts of the Paleothetys as long ago as the Carboniferous, arguing in favor of a rather old origin for the distinctive Indian mantle signature [*Zhang et al.*, 2005].

4.2.2. Mixing Model

[46] Several models have been proposed to account for the distinctive isotopic signature of Indian MORB. *Hamelin and Allègre* [1985] were the first to point out the requirement of more than two distinct end-member components in the Indian mantle source. There is still controversy concerning the nature of these components, but three are generally considered: (1) a high $^{143}Nd/^{144}Nd$, low $^{87}Sr/^{86}Sr$, relatively low $^{206}Pb/^{204}Pb$ depleted mantle

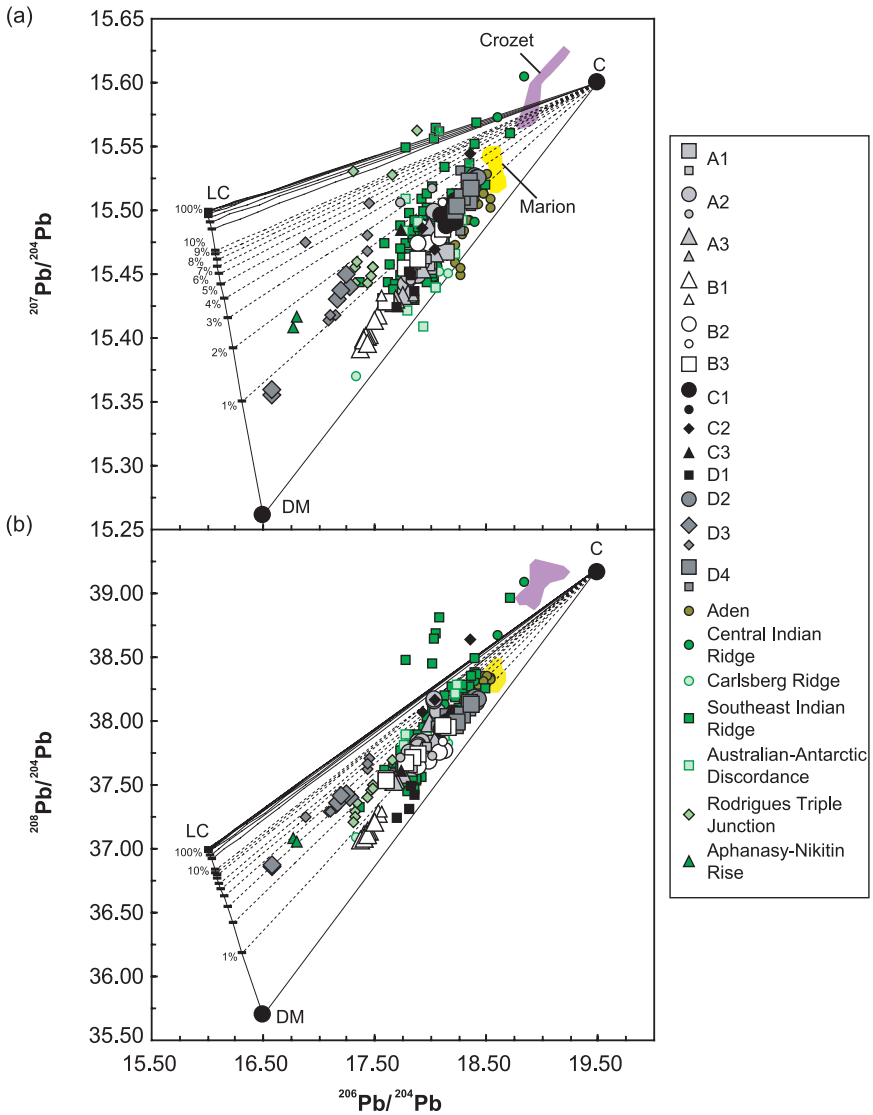

Figure 15. SWIR (a) $^{207}Pb/^{204}Pb$ and (b) $^{208}Pb/^{204}Pb$ versus $^{206}Pb/^{204}Pb$ variations, along with those of other mid-Indian Ocean ridges (See Auxiliary Material for references used). Also shown are the compositions of the three end-members (LC, lower crust; C, common component; DM, depleted mantle) as well as modeled mixing lines. The isotopic composition for the C component is taken from *Douglass and Schilling* [2000]. The lower crust composition is $^{206}Pb/^{204}Pb = 16.00$; $^{207}Pb/^{204}Pb = 15.50$; $^{208}Pb/^{204}Pb = 37.00$; $^{87}Sr/^{86}Sr = 0.70800$; $^{143}Nd/^{144}Nd = 0.511600$; Sr = 421 ppm; Nd = 21; and Pb = 2.58. Sr and Pb elemental contents are from *Rudnick and Fountain* [1995]. The Nd elemental content is in the range of those observed for granulite xenoliths (average: 17.3 ± 13, N = 133). The DM composition is $^{206}Pb/^{204}Pb = 16.50$; $^{207}Pb/^{204}Pb = 15.26$; $^{208}Pb/^{204}Pb = 35.70$; $^{87}Sr/^{86}Sr = 0.701659$; $^{143}Nd/^{144}Nd = 0.513481$; Sr = 13 ppm; Nd = 0.7; and Pb = 0.044. Marks on the mixing lines between depleted mantle and lower crust are graduated from 1 to 10%, then from 10 to 100%.

component equivalent to Central Atlantic/Pacific depleted mantle; (2) an Indian oceanic island-type mantle with moderate $^{206}Pb/^{204}Pb$, high $^{208}Pb/^{204}Pb$, $^{87}Sr/^{86}Sr$, and low $^{143}Nd/^{144}Nd$, similar to the "C" component of *Hanan and Graham* [1997]; and (3) a low $^{206}Pb/^{204}Pb$ component with relatively high $^{208}Pb/^{204}Pb$, $^{87}Sr/^{86}Sr$ and low $^{143}Nd/^{144}Nd$.

[47] Mixing models for the Indian Ocean usually appeal to these three components in two stage mixing events, in which the asthenosphere experienced widespread contamination by the low $^{206}Pb/^{204}Pb$ component, before being mixed with OIB type material [e.g., *Hamelin et al.*, 1986, *Escrig et al.*, 2004; *Douglas and Schilling*, 2000]. One variant of such a model is that of

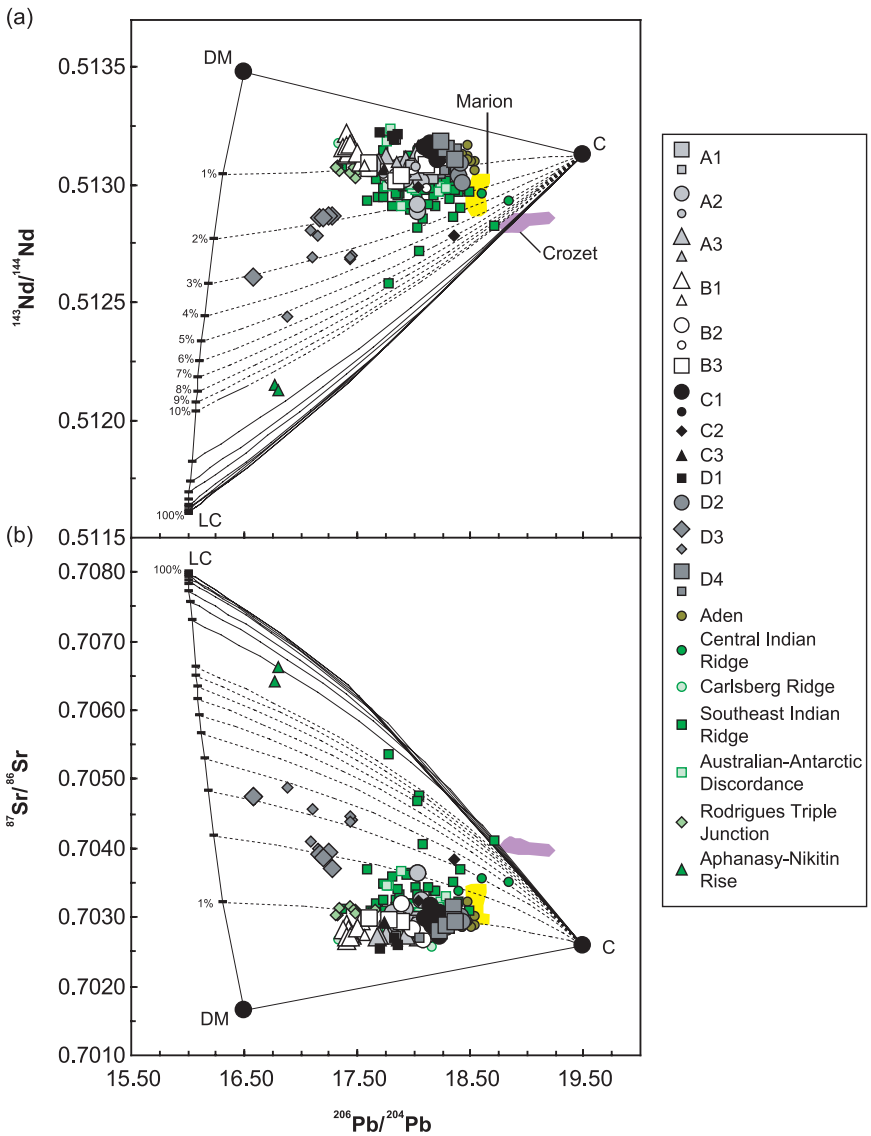

Figure 16. SWIR (a) $^{143}Nd/^{144}Nd$ and (b) $^{87}Sr/^{86}Sr$ versus $^{206}Pb/^{204}Pb$ variations, along with those of other mid-Indian Ocean ridges. Symbols as in Figure 15.

proposed by *Barling et al.* [1994], in which the entire north Atlantic and Pacific array mixes with a small amount of low $^{206}Pb/^{204}Pb$ material arising from, in their model, subcontinental lithospheric mantle. We also propose a two-stage, three component mixing model, involving a low $^{206}Pb/^{204}Pb$ component, a depleted Pacific/Central Atlantic mantle and the C component of *Douglas and Schilling* [2000] (Figures 15 and 16). The common component (C) is required to extend the Indian MORB mixing array toward high $^{206}Pb/^{204}Pb$ and may be provided by numerous plumes in the Indian Ocean (Marion, Crozet, Reunion and Amsterdam). As discussed above, we argue that the origin of the low $^{206}Pb/^{204}Pb$ component lies in material derived from the lower continental crust, which has been delaminated and injected into the mantle during ancient convergent processes.

[48] Approximately 0.5–3% of recycled lower crust is sufficient to explain the Indian Ocean population in general, while a maximum contribution of ~6% is required to account for the composition of the 39–41°E section. Although this model can account for most of the isotopic features of Indian MORB, the trends defined by the Aphanasy-Nikitin Rise require much larger amounts of lower crustal component (Figures 15 and 16). These features may be explained if the low $^{206}Pb/^{204}Pb$ component is more heterogeneous in

terms of $^{207}Pb/^{204}Pb$, $^{143}Nd/^{144}Nd$ and $^{87}Sr/^{86}Sr$ than in $^{208}Pb/^{204}Pb$, a conclusion consistent with the isotopic attributes of African granulite xenoliths (Figures 13 and 14).

5. Conclusions

[49] Sr-Nd-Pb isotope systematics for SWIR MORB dredged between 35 and 69°E reveal significant heterogeneity of the SWIR mantle over a wide range of length scales. Important isotopic variations occur on local scales, independently of ridge segmentation, which are generally of greater amplitude than those observed on larger scales. The existence of such small scale isotopic domains demonstrate that there has been no vigorous, widespread and long-term convection inducing mantle mixing, and that magma mixing given the present sampling has been restricted to a scale of ~308 km.

[50] Our new data for lavas from the deep easternmost SWIR domain confirm that they differ isotopically from those of the Rodrigues Triple Junction, Southeast Indian Ridge and Central Indian Ridge indicating the existence of an abrupt boundary occurring over an on-axis distance of less than ~78 km.

[51] Our new results for lavas from the 39–41°E section, which are considered to represent one of the best indicators of the material responsible for the distinctive Indian mantle signature exhibit the lowest $^{206}Pb/^{204}Pb$ values (to 16.58) yet found among oceanic islands and spreading centers worldwide and confirm their extremely high $^{87}Sr/^{86}Sr$, $^{207}Pb/^{204}Pb$, $^{208}Pb/^{204}Pb$ and low $^{143}Nd/^{144}Nd$. These lavas do not bear any affinity with modern lavas from the nearby Marion hot spot. They also cannot be accounted for by the presence in the source of old sedimentary material, as no present-day group of sediment has parent-daughter attributes (e.g., variable U/Pb and constant Th/Pb) similar to those of these lavas, even when dewatering processes are considered. Mixture of old subduction modified mantle with a depleted mantle source of Pacific affinity give not rise to sufficiently high $^{208}Pb/^{204}Pb$ and $^{207}Pb/^{204}Pb$ to explain the isotopic features of these lavas. Our preferred interpretation is that the isotopic attributes of this section (low $^{206}Pb/^{204}Pb$, $^{143}Nd/^{144}Nd$ and high $^{207}Pb/^{204}Pb$, $^{208}Pb/^{204}Pb$) are the result of the presence of stranded lower continental crust embedded in the upper mantle, which has been possibly detached and incorporated during convergent processes.

[52] At a global scale, most of the isotopic attributes of Indian MORB can be accounted by a two stage three component mixing model involving a depleted mantle of Central Atlantic/Pacific affinity, the common component (C) and a fertile low $^{206}Pb/^{204}Pb$ component, arising from the lower crust.

Acknowledgments

[53] We are grateful to Tod Waight, Olivier Rouxel, and Laurie Reisberg for assistance with the analytical work and fruitful discussions at CRPG and DLC. We also thank Mathilde Cannat. Funding was provided by CNRS-INSU, Programme Dorsale and a Marie Curie fellowship (HPMF-CT-2001-01427). The IFRTP provided access to the Marion Dufresne II for sampling. David Christie and Rex Taylor are gratefully acknowledged for their constructive reviews that helped to improve the manuscript, which also benefited from editorial comments of William White and Daniel Sauter.

References

Allègre, C. J., B. Hamelin, and B. Dupré (1984), Statistical analysis of isotopic ratios in MORB: The mantle blob cluster model and the convective regime of the mantle, *Earth Planet. Sci. Lett.*, *71*, 71–84.

Arndt, N. T., and U. Christensen (1992), The role of lithospheric mantle in continental flood volcanism: Thermal and geochemical constraints, *J. Geophys. Res.*, *97*, 10,967–10,981.

Arndt, N. T., and S. L. Goldstein (1989), An open boundary between lower continental crust and mantle: Its role in crust formation and crustal recycling, *Tectonophysics*, *161*, 201–212.

Arndt, N. T., G. K. Czamanske, J. L. Wooden, and V. A. Fedorenko (1993), Mantle and crustal contributions to continental flood volcanism, *Tectonophysics*, *223*, 39–52.

Baker, J. A., D. Peate, T. Waight, and C. M. Meyzen (2004), Pb isotopic analysis of standards using a ^{207}Pb-^{204}Pb double spike and thallium to correct for mass bias with a double focusing MC-ICP-MS, *Chem. Geol.*, *211*, 275–303.

Barling, J., S. L. Goldstein, and I. A. Nicholls (1994), Geochemistry of Heard Island (southern Indian Ocean): Characterization of an enriched mantle component and geochemical constraints, *J. Petrol.*, *35*, 1017–1053.

Ben Othman, D., W. M. White, and P. J. Patchett (1989), The geochemistry of marine sediments, island arc magma genesis, and crust-mantle recycling, *Earth Planet. Sci. Lett.*, *94*, 1–21.

Cannat, M., C. Rommevaux-Jestin, D. Sauter, C. Deplus, and V. Mendel (1999), Formation of the axial relief at the very slow spreading Southwest Indian Ridge (49°–69°E), *J. Geophys. Res.*, *104*, 22,825–22,844.

Carlson, R. W., and A. J. Irving (1994), Depletion and enrichment history of the subcontinental lithospheric mantle: An Os, Sr, Nd and Pb isotopic study of ultramafic xenoliths from the northwestern Wyoming craton, *Earth Planet. Sci. Lett.*, *126*, 457–472.

Chauvel, C., and J. Blichert-Toft (2001), A hafnium isotope and trace element perspective on melting of the depleted mantle, *Earth Planet. Sci. Lett.*, *190*(3–4), 137–151.

Chu, D., and R. Gordon (1999), Evidence for motion between Nubia and Somalia along the Southwest Indian Ridge, *Nature*, *398*, 64–67.

Class, C., D. M. Miller, S. L. Goldstein, and C. H. Langmuir (1999), Distinguishing melt and fluid subduction components in Umnak volcanics, Aleutian arc, *Geochem. Geophys. Geosyst.*, *1*(6), doi:10.1029/1999GC000010.

Cohen, R. S., R. K. O'Nions, and J. B. Dawson (1984), Isotope geochemistry of xenoliths from East Africa: Implications for development of mantle reservoirs and their interaction, *Earth Planet. Sci. Lett.*, *68*, 209–220.

Collins, W. J. (2003), Slab pull, mantle convection, and Pangaean assembly and dispersal, *Earth Planet. Sci. Lett.*, *205*, 225–237.

Currey, J. R., and T. Munasinghe (1991), Origin of the Rajmahal Traps and the 85°E Ridge: Preliminary reconstructions of the trace of the Crozet Hotspot, *Geology*, *19*, 1237–1240.

Dosso, L., H. Bougault, P. Beuzard, J. Y. Calvez, and J. L. Loron (1988), The geochemical structure of the Southeast Indian Ridge, *Earth Planet. Sci. Lett.*, *88*, 47–59.

Douglass, J., and J.-G. Schilling (2000), Systematics of three-component, pseudo-binary mixing lines in 2D isotope ratio space representations and implications for mantle-plume ridge interactions, *Chem. Geol.*, *163*, 1–23.

Douglass, J., J.-G. Schilling, and D. Fontignie (1999), Plume-ridge interactions of the Discovery and Shona mantle plumes with the southern mid-Atlantic ridge (40 degrees–55 degrees S), *J. Geophys. Res.*, *104*, 2941–2962.

Downes, H., A. J. W. Markwick, P. D. Kempton, and M. F. Thirlwall (2001), The lower crust beneath cratonic north-east Europe: Isotopic constraints from garnet granulite xenoliths, *Terra Nova*, *13*, 395–400.

Dunn, T., and C. Sen (1994), Mineral/matrix partition coefficients for orthopyroxene, plagioclase, and olivine in basaltic to andesitic systems: A combined analytical and experimental study, *Geochim. Cosmochim. Acta*, *58*, 717–733.

Dunstan, L. P., J. W. Gramlich, and I. L. Barnes (1980), Absolute isotopic abundance and the atomic weight of a reference sample of Thallium, *J. Res. Natl. Bur. Stand. U.S.*, *85*, 1–10.

Dupré, B., and C. Allègre (1983), Pb-Sr isotope variation in Indian Ocean basalts and mixing phenomena, *Nature*, *303*, 142–146.

Escrig, S., F. Capmas, B. Dupré, and C. J. Allègre (2004), Osmium isotopic constraints on the nature of the DUPAL anomaly from Indian mid-ocean-ridge basalts, *Nature*, *431*, 59–63.

Francis, T. G. J., and R. W. Raitt (1967), Seismic refraction measurements in the southern Indian Ocean, *J. Geophys. Res.*, *72*, 3015–3041.

Galer, S. J., A. W. Abouchami, and J. D. Macdougall (1999), East Pacific Rise MORB through the Pb-isotope looking glass, *Eos Trans. AGU*, *80*(46), Fall Meet. Suppl., F1086.

George, R., S. Turner, C. Hawkesworth, J. Morris, C. Nye, J. Ryan, and S. Zheng (2003), Melting processes and fluid and sediment transport rates along the Alaska-Aleutian arc from an integrated U-Th-Ra-Be isotope study, *J. Geophys. Res.*, *108*(B5), 2252, doi:10.1029/2002JB001916.

George, R. M., S. P. Turner, C. J. Hawkesworth, C. R. Bacon, C. J. Nye, P. Stelling, and S. T. Dreher (2004), Chemical versus temporal controls on the evolution of tholeitic and calc-alkaline magmas at two volcanoes in the Alaska-Aleutian arc, *J. Petrol.*, *45*, 203–219.

Georgen, J. E., and J. Lin (2002), Three-dimensional passive flow and temperature structure beneath oceanic ridge-ridge-ridge triple junctions, *Earth Planet. Sci. Lett.*, *204*, 115–132.

Georgen, J., and J. Lin (2003), Plume-transform interaction at ultra-slow spreading ridges: Implications for the Southwest Indian Ridge, *Geochem. Geophys. Geosyst.*, *4*(9), 9106, doi:10.1029/2003GC000542.

Georgen, J. E., J. Lin, and H. J. B. Dick (2001), Evidence from gravity anomalies for interactions of the Marion and Bouvet hotpots with the Southwest Indian Ridge: Effects of transform offsets, *Earth Planet. Sci. Lett.*, *187*, 283–300.

Georgen, J. E., M. D. Kurz, H. J. B. Dick, and J. Lin (2003), Low $^{3}He/^{4}He$ ratios in basalt glasses from the western Southwest Indian Ridge (10°–24°E), *Earth Planet. Sci. Lett.*, *206*, 509–528.

Hamelin, B., and C. Allègre (1985), Large scale regional units in the depleted upper mantle revealed by an isotope study of the Southwest Indian Ridge, *Nature*, *315*, 196–199.

Hamelin, B., B. Dupré, and C. J. Allègre (1986), Pb-Sr-Nd isotopic data of Indian Ocean Ridges: New evidence of large-scale mapping of mantle heterogeneities, *Earth Planet. Sci. Lett.*, *76*, 288–298.

Hanan, B. B., and D. W. Graham (1997), Lead and helium isotope evidence from oceanic basalts for a common deep source of mantle plume, *Science*, *272*, 991–995.

Hanan, B. B., J. Blichert-Toft, D. G. Pyle, and D. M. Christie (2004), Contrasting origins of the upper mantle revealed by hafnium and lead isotopes from the Southeast Indian Ridge, *Nature*, *432*, 91–94.

Hart, S. R. (1984), A large-scale isotope anomaly in the Southern Hemisphere mantle, *Nature*, *309*, 753–757.

Hart, S. R. (1988), Heterogeneous mantle domains: Signatures, genesis and mixing chronologies, *Earth Planet. Sci. Lett.*, *90*, 273–296.

Hawkesworth, C. J., A. J. Erlank, P. D. Kempton, and F. G. Waters (1990), Mantle metasomatism: Isotope and trace element trends in xenoliths from Kimberley, South Africa, *Chem. Geol.*, *85*, 19–34.

Hergt, J. M., and C. J. Hawkesworth (1994), The Pb, Sr, and Nd evolution of the Lau Basin: Implication for mantle dynamics during backarc opening, *Proc. Ocean Drill. Program Sci. Results*, *135*, 505–517.

Hofmann, A. W. (2003), Sampling mantle heterogeneity through oceanic basalts: Isotopes and trace elements, in *The Mantle and Core*, edited by R. W. Carlson, vol. 2, *Treatise on Geochemistry*, edited by H. Holland and K. K. Turekian, pp. 61–101, Elsevier, New York.

Hofmann, A. W., and W. M. White (1982), Mantle plumes from ancient oceanic crust, *Earth Planet. Sci. Lett.*, *57*, 421–436.

Holm, P. M. (2002), Sr, Nd and Pb isotopic composition of in situ lower crust at the Southwest Indian Ridge: Results from ODP Leg 176, *Chem. Geol.*, *184*, 195–216.

Huang, Y. M., P. VanCalsteren, and C. J. Hawkesworth (1995), The evolution of the lithosphere in southern Africa: A perspective on the basic granulite xenoliths from kimberlites in South Africa, *Geochim. Cosmochim. Acta*, *59*, 4905–4920.

Ito, E., W. M. White, and C. Göpel (1987), The O, Sr, Nd and Pb isotope geochemistry of MORB, *Chem. Geol.*, *62*, 157–176.

Jull, M., and P. B. Kelemen (2001), On the conditions for lower crustal convective instability, *J. Geophys. Res.*, *106*, 6423–6446.

Kamenetsky, V. S., R. Maas, N. M. Sushchevskaya, M. D. Norman, I. Cartwright, and A. A. Peyve (2001), Remnants of Gondwanan continental lithosphere in oceanic upper mantle: Evidence from the South Atlantic Ridge, *Geology*, *29*, 243–246.

Kay, R. W., and S. M. Kay (1993), Delamination and delamination magmatism, *Tectonophysics*, *219*, 177–189.

Kempton, P. D., C. J. Hawkesworth, and M. Fowler (1991), Geochemistry and isotopic composition of gabbros from layer 3 of the Indian Ocean crust, hole 735B, in *Proc. Ocean Drill. Program Sci. Results*, *118*, 127–144.

Kempton, P. D., J. A. Pearce, T. L. Barry, J. G. Fitton, C. Langmuir, and D. M. Christie (2002), Sr-Nd-Pb-Hf isotope results from ODP Leg 187: Evidence for mantle dynamics of the Australian-Antarctic Discordance and origin of the Indian MORB source, *Geochem. Geophys. Geosyst.*, *3*(12), 1074, doi:10.1029/2002GC000320.

Kinzler, R. J., and T. L. Grove (1992), Primary magmas of mid-ocean ridge basalts: 2. Applications, *J. Geophys. Res.*, *97*, 6907–6926.

Klein, E. M., and C. H. Langmuir (1987), Global correlations of ocean ridge basalt chemistry with axial depth and crustal thickness, *J. Geophys. Res.*, *92*, 8089–8115.

Klein, E. M., C. H. Langmuir, A. Zindler, H. Staudigel, and B. Hamelin (1988), Isotope evidence of mantle convection boundary at the Australian-Antarctic Discordance, *Nature*, *333*, 623–629.

Kramers, J. D. (1977), Lead and strontium isotopes in cretaceous kimberlites and mantle-derived xenoliths from Southern Africa, *Earth Planet. Sci. Lett.*, *34*, 419–431.

Kramers, J. D., and I. N. Tolstikhin (1997), Two terrestrial lead isotope paradoxes, forward transport modelling, core formation and the history of the continental crust, *Chem. Geol.*, *139*, 75–110.

Kramers, J. D., J. C. M. Roddick, and J. B. Dawson (1983), Trace element and isotope studies on veined, metasomatic and "MARID" xenoliths from Bultfontein, South Africa, *Earth Planet. Sci. Lett.*, *65*, 90–106.

Langmuir, C. H., and J. F. Bender (1984), The geochemistry of oceanic basalts in the vicinity of transform faults—Observations and implications, *Earth Planet. Sci. Lett.*, *69*, 107–127.

Langmuir, C. H., E. M. Klein, and T. Plank (1992), Petrological systematics of mid-ocean ridge basalts: Constraints on melt generation beneath Ocean ridges, in *Mantle Flow and Melt Generation at Mid-Ocean Ridges*, *Geophys. Monogr. Ser.*, vol. 71, edited by J. Phipps-Morgan, D. K. Blackmann, and J. M. Sinton, pp. 183–280, AGU, Washington, D. C.

LeRoex, A. P., H. J. B. Dick, and R. L. Fisher (1989), Petrology and geochemistry of MORB from 25°E to 46°E along the Southwest Indian Ridge: Evidence for contrasting style of mantle enrichment, *J. Petrol.*, *30*, 947–986.

Luais, B., P. Télouk, and F. Albarède (1997), Precise and accurate neodymium isotopic measurements by plasma-source mass spectrometry, *Geochim. Cosmochim. Acta*, *61*, 4847–4854.

Machado, N., J. N. Ludden, C. Brooks, and G. Thompson (1982), Fine-scale isotopic heterogeneity in the sub-Atlantic mantle, *Nature*, *295*, 226–228.

Mahoney, J. J., J. H. Natland, W. M. White, R. Poreda, and S. H. Bloomer (1989), Isotopic and geochemical provinces of the Indian Ocean spreading centers, *J. Geophys. Res.*, *94*, 4033–4052.

Mahoney, J., C. Nicollet, and C. Dupuy (1991), Madagascar basalts: Tracking oceanic and continental sources, *Earth Planet. Sci. Lett.*, *104*, 350–363.

Mahoney, J., A. P. LeRoex, Z. Peng, R. L. Fisher, and J. H. Natland (1992), Southwestern limits of Indian ocean ridge mantle and origin of low $^{206}Pb/^{204}Pb$ mid-ocean ridge basalt: Isotope systematics of the Central Southwest Indian Ridge (17–50°E), *J. Geophys. Res.*, *97*, 19,771–19,790.

Mahoney, J. J., W. M. White, B. G. J. Upton, C. R. Neal, and R. A. Scrutton (1996), Beyond EM-1: Lavas from Afanasy-Nikitin Rise and the Crozet Archipelago, Indian Ocean, *Geology*, *24*, 615–618.

Mahoney, J. J., R. Freï, M. L. G. Tejada, and T. F. Nägler (1998), Tracing the Indian Ocean mantle domain through time: Isotopic results from old west Indian, East Thetyan, and South Pacific seafloor, *J. Petrol.*, *39*, 1285–1306.

Mahoney, J. J., D. W. Graham, D. M. Christie, K. T. M. Johnson, L. S. Hall, and L. Vonderhaar (2002), Between a hotspot and a cold Spot: Isotopic variations in the Southeast Indian Ridge asthenosphere, 86E-118E, *J. Petrol.*, *43*, 1155–1176.

Manhès, G., J. F. Minster, and C. J. Allègre (1978), Comparative uranium-thorium-lead and rubidium-strontium study of the Saint Séverin amphotérite: Consequences for early solar system chronology, *Earth Planet. Sci. Lett.*, *39*, 14–24.

Marks, K. M., and A. A. Tikku (2001), Cretaceous reconstructions of East Antarctica, Africa and Madagascar, *Earth Planet. Sci. Lett.*, *186*, 479–495.

McDade, P., B. J. Wood, and J. D. Blundy (2003), Near solidus trace element partitioning between Tinaquillo lherzolithe and melt at 1.5 GPa, *Phys. Earth Planet. Inter.*, *139*, 129–147.

McKenzie, D. P., and M. Bickle (1988), The volume and composition of melt generated by extension of the lithosphere, *J. Petrol.*, *25*, 625–679.

McKenzie, D. P., and R. K. O'Nions (1991), Partial melts distributions from inversion of rare earth element concentrations, *J. Petrol.*, *32*, 1021–1091.

Mendel, V., D. Sauter, L. M. Parsey, and J. R. Vaney (1997), Segmentation and morphotectonic variations along an ultra-slow spreading center: The Southwest Indian Ridge (57°E–70°E), *Mar. Geophys. Res.*, *19*, 505–553.

Mendel, V., D. Sauter, C. Rommevaux-Jestin, P. Patriat, F. Lefebvre, and L. M. Parson (2003), Magmato-tectonic cyclicity at the ultra-slow spreading Southwest Indian Ridge: Evidence from variations of axial volcanic ridge morphology and abyssal hills pattern, *Geochem. Geophys. Geosyst.*, *4*(5), 9102, doi:10.1029/2002GC000417.

Meyzen, C. M., M. J. Toplis, E. Humler, J. N. Ludden, and C. Mével (2003), A discontinuity in mantle composition beneath the Southwest Indian Ridge, *Nature*, *421*, 731–733.

Michard, A. R., R. Montigny, and R. Schlich (1986), Geochemistry of the mantle beneath the Rodriguez triple junction and the Southeast Indian ridge, *Earth Planet. Sci. Lett.*, *78*, 104–114.

Miller, D. M., S. L. Goldstein, and C. H. Langmuir (1994), Cerium/lead and lead isotope ratios in arc magmas and the enrichment of lead in the continents, *Nature*, *368*, 514–520.

Minshull, T. A., and R. S. White (1996), Thin crust on the flanks of the slow-spreading Southwest Indian Ridge, *Geophys. J. Int.*, *125*, 139–148.

Mitchell, N. C. (1991), Distributed extension at the Indian Ocean Triple Junction, *J. Geophys. Res.*, *96*, 8019–8043.

Müller, M. R., C. J. Robinson, T. A. Minshull, R. S. White, and M. J. Bickle (1997), Thin crust beneath ocean drilling program borehole 735 B at the Southwest Indian ridge?, *Earth Planet. Sci. Lett.*, *148*, 93–107.

Müller, M. R., T. A. Minshull, and R. S. White (1999), Segmentation and melt supply at the Southwest Indian Ridge, *Geology*, *27*, 867–870.

Müller, M. R., T. A. Minshull, and R. S. White (2000), Crustal structure of the Southwest Indian Ridge at the Atlantis II Fracture Zone, *J. Geophys. Res.*, *105*, 25,809–25,828.

Müller, R. D., J.-Y. Royer, and L. A. Lawver (1993), Revised plate motions relative to the hotspots from Atlantic and Indian ocean hotpot tracks, *Geology*, *21*, 275–278.

Nägler, T. F., and J. D. Kramers (1998), Nd isotopic evolution of the upper mantle during the Precambrian: Models, data and the uncertainty of both, *Precambrian Res.*, *91*, 233–252.

Niu, Y., K. D. Collerson, R. Batiza, J. I. Wendt, and M. Regelous (1999), Origin of enriched-type mid-ocean ridge basalt at ridges far from mantle plumes: The East Pacific Rise at 11°20′N, *J. Geophys. Res.*, *104*, 7067–7087.

Parson, L., D. Sauter, V. Mendel, P. Patriat, and R. Searle (1997), Evolution of the axial geometry of the Southwest Indian Ocean Ridge between the Melville Fracture Zone and the Indian Ocean Triple Junction—Implications for segmentation on very slow-spreading ridges, *Mar. Geophys. Res.*, *19*, 535–552.

Patriat, P., and J. Segouffin (1988), Reconstruction of the central Indian Ocean, *Tectonophysics*, *155*, 211–234.

Patriat, P., D. Sauter, M. Munschy, and L. Parson (1997), A survey of the Southwest Indian Ridge axis between Atlantis II Fracture Zone and the Indian Ocean Triple Junction: Regional setting and large scale segmentation, *Mar. Geophys. Res.*, *19*, 457–480.

Pearson, D. G., and G. M. Nowell (2002), The continental lithospheric mantle: Characteristics and significance as a mantle reservoir, *Philos. Trans. R. Soc. London, Ser. A*, *360*(1800), 2383–2410.

Plank, T., and C. H. Langmuir (1988), An evaluation of the global variations in the major element chemistry of arc basalts, *Earth Planet. Sci. Lett.*, *90*, 349–370.

Plank, T., and C. H. Langmuir (1998), The chemical composition of subducting sediments and its consequences for the crust and mantle, *Chem. Geol.*, *145*, 325–394.

Price, R. C., A. K. Kennedy, M. Riggs-Sneeringer, and F. A. Frey (1986), Geochemistry of basalts from the Indian Ocean triple junction: Implications for the generation and evolution of Indian Ocean Ridge basalts, *Earth Planet. Sci. Lett.*, *78*, 379–396.

Pyle, D. G., D. M. Christie, and J. J. Mahoney (1992), Resolving an isotopic boundary within the Australian-Antarctic Discordance, *Earth Planet. Sci. Lett.*, *112*(1–4), 161–178.

Pyle, D. G., D. M. Christie, J. J. Mahoney, and R. A. Duncan (1995), Geochemistry and geochronology of ancient southeast Indian and southwest Pacific seafloor, *J. Geophys. Res.*, *100*(B11), 22,261–22,282.

Rehkämper, M., and A. W. Hofmann (1997), Recycled ocean crust and sediment in Indian Ocean MORB, *Earth Planet. Sci. Lett.*, *147*, 93–106.

Rehkämper, M., and K. Mezger (2000), Investigation of matrix effects for Pb isotope ratio measurements by multiple collector ICP-MS: Verification and application of optimised analytical protocols, *J. Anal. Atom. Spectrom.*, *15*, 1451–1460.

Robinson, C. J., M. J. Bickle, T. A. Minshull, R. S. White, and A. R. L. Nichols (2001), Low degree melting under the Southwest Indian Ridge: The roles of mantle temperature, conductive cooling and wet melting, *Earth Planet. Sci. Lett.*, *188*, 383–398.

Rommevaux-Jestin, C., C. Deplus, and P. Patriat (1997), Mantle Bouguer anomaly along an ultra-slow spreading ridge: Implications for accretionary processes and comparison with results from Central Mid-Atlantic Ridge, *Mar. Geophys. Res.*, *19*, 481–503.

Royer, J. Y., P. Patriat, H. W. Bergh, and C. R. Scotese (1988), Evolution of the Southwest Indian Ridge from the late cretaceous (anomaly 34) to the Middle Eocene (anomaly 20), *Tectonophysics*, *155*, 235–260.

Rudnick, R. L., and D. M. Fountain (1995), Nature and composition of the continental crust: A lower crustal perspective, *Rev. Geophys.*, *33*, 267–309.

Rudnick, R. L., and S. L. Goldstein (1990), The Pb isotopic compositions of lower crustal xenoliths and the evolution of lower crustal Pb, *Earth Planet. Sci. Lett.*, *98*, 192–207.

Saal, A. E., S. R. Hart, N. Shimizu, E. H. Hauri, and G. D. Layne (1998), Pb isotopic variability in melt inclusions from oceanic island basalts, Polynesia, *Science*, *282*, 1481–1484.

Salters, J. M., and H. J. B. Dick (2002), Mineralogy of the mid-ocean-ridge basalt source from neodymium isotopic composition in abyssal peridotites, *Nature*, *418*, 68–72.

Sauter, D., P. Patriat, C. Rommevaux-Jestin, M. Cannat, A. Briais, and Gallieni Shipboard Scientific Party (2001), The Southwest Indian Ridge between 49°15′E and 57°E: Focused accretion and magma redistribution, *Earth Planet. Sci. Lett.*, *192*, 303–317.

Schiano, P., J. L. Birck, and C. J. Allègre (1997), Osmium-strontium-neodymium-lead isotopic covariations in mid-ocean ridge basalt glasses and the heterogeneity of the upper mantle, *Earth Planet. Sci. Lett.*, *150*, 363–379.

Schilling, J. G., R. H. Kingsley, B. H. Hanan, and B. L. McCully (1992), Nd-Sr-Pb isotopic variations along the Gulf of Aden: Evidence for Afar mantle plume-continental lithosphere interaction, *J. Geophys. Res.*, *97*, 10,927–10,966.

Schilling, J.-G., R. Kingsley, D. Fontignie, R. Poreda, and S. Xue (1999), Dispersion of the Jan Mayen and Iceland mantle plumes in the arctic: A He-Pb-Nd-Sr isotope tracer study of basalts from the Kolbeinsey, Mohns, and Knipovich Ridges, *J. Geophys. Res.*, *104*, 10,543–10,569.

Schmitz, M. D., and S. A. Bowring (2000), The significance of U-Pb zircon dates in lower crustal xenoliths from the southwestern margin of the Kaapvaal craton, southern Africa, *Chem. Geol.*, *172*, 59–76.

Sclater, J. G., R. L. Fisher, P. Patriat, C. Tapscott, and B. Parsons (1981), Eocene to recent development of the South West Indian Ridge, a consequence of the evolution of the Indian Ocean Triple Junction, *Geophys. J. R. Astron. Soc.*, *64*, 587–604.

Shen, Y., and D. Forsyth (1995), Geochemical constraints on initial and final depths of melting beneath mid-ocean ridges, *J. Geophys. Res.*, *100*, 2211–2237.

Shinjo, R., J. D. Woodhead, and J. M. Hergt (2000), Geochemical variation within the northern Ryukyu Arc: Magma source compositions and geodynamic implications, *Contrib. Mineral. Petrol.*, *140*, 263–282.

Smith, S. E., J. F. Casey, W. B. Bryan, L. Dmitriev, S. Silantyev, and R. Magakyan (1998), Geochemistry of basalts from the Hayes Transform region of the mid-Atlantic Ridge, *J. Geophys. Res.*, *103*, 5305–5329.

Smith, W. H. F., and D. T. Sandwell (1997), Global seafloor topography from satellite altimetry and ship depth soundings, *Science*, *277*, 1957–1962.

Storey, M., A. D. Saunders, J. Tarney, I. L. Gibson, M. J. Norry, M. F. Thirlwall, P. Leat, R. N. Thompson, and M. A. Menzies (1989), Contamination of Indian Ocean asthenosphere by the Kerguelen Heard mantle plume, *Nature*, *338*, 574–576.

Storey, M., J. J. Mahoney, A. D. Saunders, R. A. Duncan, S. P. Kelley, and M. F. Coffin (1995), Timing of hotspot-related volcanism and the break-up of Madagascar and India, *Science*, *267*, 852–855.

Storey, M., J. J. Mahoney, and A. D. Saunders (1997), Cretaceous basalts in Madagascar and the transition between plume and continental lithosphere mantle source, in *Large Igneous Provinces: Continental, Oceanic, and Planetary Flood Volcanism*, *Geophys. Monogr. Ser.*, vol. 100, edited

by J. J. Mahoney and M. F. Coffin, pp. 95–122, AGU, Washington, D. C.

Stracke, A., M. Bizimis, and V. J. M. Salters (2003), Recycling oceanic crust: Quantitative constraints, *Geochem. Geophys. Geosyst.*, *4*(3), 8003, doi:10.1029/2001GC000223.

Sturm, M. E., E. M. Klein, D. W. Graham, and J. L. Karsten (1999), Age constraints on crustal recycling to the mantle beneath the Southern Chile Ridge: He-Pb-Sr-Nd isotope systematics, *J. Geophys. Res.*, *104*, 5097–5114.

Tapscott, C., P. Patriat, R. L. Fisher, J. G. Sclater, H. Hoskins, and B. Parsons (1980), The Indian Ocean Triple Junction, *J. Geophys. Res.*, *85*, 4723–4739.

Todt, W., R. A. Cliff, A. Hanser, and A. W. Hofmann (1996), Evaluation of a ^{202}Pb-^{205}Pb double spike for high-precision lead isotope analysis, in *Earth Processes: Reading the Isotopic Code*, *Geophys. Monogr. Ser.*, vol. 95, edited by A. Basu and S. R. Hart, pp. 429–437, Washington, D. C.

Turcotte, D. L. (1989), Dynamics of recycling, in *Crust/Mantle Recycling at Convergence Zones*, edited by S. R. Hart and L. Gülen, *NATO ASI Ser., Ser. C*, *258*, 245–257.

Weaver, B. L. (1991), The origin of ocean basalt end-member compositions: Trace element and isotopic constraints, *Earth Planet. Sci. Lett.*, *104*, 381–397.

Wendt, J. I., M. Regelous, Y. Niu, R. Hekinian, and K. D. Collerson (1999), Geochemistry of lavas from the Garrett Transform Fault: Insights into mantle heterogeneity beneath the eastern Pacific, *Earth Planet. Sci. Lett.*, *173*, 271–284.

West, B. P., H. Fujimoto, C. Honko, K. Tamaki, and J. C. Sempéré (1995), A three dimensional gravity study of the Rodriguez Triple Junction and the South-East Indian Ridge, *Earth Planet. Sci. Lett.*, *133*, 175–184.

White, W. M., A. W. Hofmann, and H. Puchelt (1987), Isotope geochemistry of Pacific mid-ocean ridge basalts, *J. Geophys. Res.*, *92*, 4881–4893.

White, W. M., F. Albarède, and P. Télouk (2000), High-precision analysis of Pb isotope ratios by multi-collector ICP-MS., *Chem. Geol.*, *167*, 257–270.

Zhang, S.-Q., J. J. Mahoney, X.-X. Mo, A. M. Ghazi, L. Milani, A. J. Crawford, T.-Y. Guo, and Z.-D. Zhao (2005), Evidence for a widespread Thetyan upper mantle with Indian-Ocean-type isotopic characteristics, *J. Petrol.*, *46*, 829–858.